Calibration of Acoustic Emission Systems for Monitoring the Metal Cutting Process

by

E. Emel
Doctoral Student

and

E. Kannatey-Asibu, Jr.
Assistant Professor

Report No. UM-MEAM-84-30

Department of Mechanical Engineering
and Applied Mechanics
The University of Michigan
Ann Arbor, MI 48109

ABSTRACT

As a step towards eliminating or minimizing possible discrepancies between acoustic emission results obtained for similar conditions, but on different systems, an efficient and reliable method for AE system calibration is under development. The technique is based on the reciprocity concept. Using a computerized set-up, calibrations obtained for conventional transducers are shown to correspond with the manufacturers calibrations. Problems to be encountered during calibration and how they can be eliminated are discussed, including modifications to existing theory which were developed for calibrations involving infinite media. Preliminary models are developed for predicting AE spectral components from macroscopic phenomenon. Visual analysis of AE signals generated during machining shows that increasing wear has a strong effect on the spectral characteristics of the signals. The present phase of the investigation will form the basis towards identification of the sources of a detected signal and their characteristics. Such an analysis will be the focus of subsequent work.

Included, as appendices, are:

a) A review of research on acoustic emission monitoring of the metal cutting process, and

b) A theoretical analysis of the rate of flank wear.

Engn
UMR
1402

1. INTRODUCTION

Tool wear sensing and tool breakage detection in real time are essential prerequisites to automation of machining processes. Undetected tool breakage can result in extensive damage to part and machinery, while down-time associated with unpredicted tool breakage can be expensive, in terms of time and cost. A knowledge of the state of tool wear at any time will enable tools to be changed economically and also impending fracture to be predicted. The relation of tool wear sensing as a sub-category of the "factory of the future" is more clearly illustrated schematically in Fig.1.

A number of techniques have been developed over the years for sensing tool wear, both off-line and in real time, but there has been no success yet in developing a sensor that is universally acceptable for all industrial applications. An excellent review of techniques developed is presented by Cook [1], Micheletti [2], Tlusty [3], and their respective co-workers.

Acoustic emission is becoming increasingly important as a method for monitoring several aspects of manufacturing processes and also in detecting system defects. Acoustic emission (AE) refers to elastic stress waves generated as a result of the rapid release of strain energy within a material due to a rearrangment of its internal structure [8]. Basic research pertaining to the use of AE in investigating fundamental aspects of the metal cutting process have been highly succesful with significant advances being made in the past few years [4-20]. Studies have illustrated the strong potential for AE not only as a tool wear sensing technique, but also for studying the mechanics of the metal cutting process [8,9,20]. However, there are still problem areas that need further investigation before the full potential of AE can be realized.

One major problem area that is the long range goal of this project is the development of effective signal processing techniques for analyzing AE signals generated during machining.

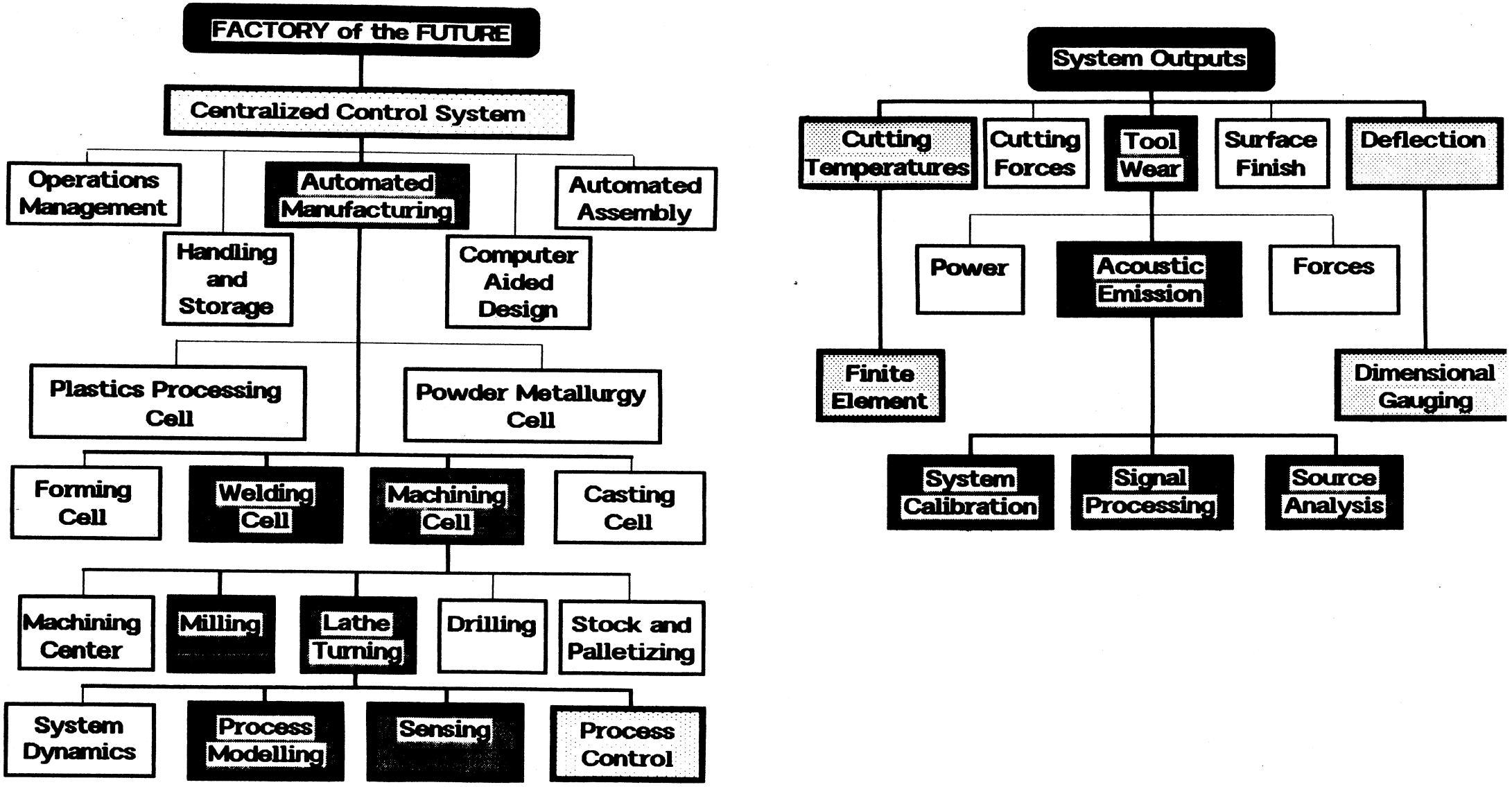
FACTORY of the FUTURE
Centralized Control System
Operations Management
Automated Manufacturing
Automated Assembly
Handling and Storage
Computer Aided Design
Plastics Processing Cell
Powder Metallurgy Cell
Forming Cell
Welding Cell
Machining Cell
Casting Cell
Machining Center
Milling
Lathe Turning
Drilling
Stock and Palletizing
System Dynamics
Process Modelling
Sensing
Process Control
System Outputs
Cutting Temperatures
Cutting Forces
Tool Wear
Surface Finish
Deflection
Power
Acoustic Emission
Forces
Finite Element
Dimensional Gauging
System Calibration
Signal Processing
Source Analysis

Figure 1.

The need for such an analysis stems from the fact that AE generated during metal cutting is from several sources [11], not all of which are directly related to tool wear, and it is necessary to distinguish wear-related signals (see Fig. 2) from other unrelated signals, if reliable information is to be obtained about the state of wear. The basic concepts to be used in this respect are extensively discussed in reference [11]. In addition to developing signal processing methods, it is also necessary to develop efficient and reliable techniques for calibrating the AE instrumentation as well as being able to interpret the results of the signal processing in terms of the process characteristics. The latter two sub-problem areas have been the focus of the research project this year.

Following is a brief review of past work on AE monitoring of the cutting process, and discussions on the preliminary concepts on source analysis modeling, as well as the calibration method being developed.

2. BACKGROUND

2.1 Acoustic Emission Source Analysis

Among the earliest studies on AE monitoring of the cutting process were the works of Iwata and Moriwaki [4], Grabec and Leskovar [5], and Dornfeld and Kannatey-Asibu [6-12]. Iwata and Moriwaki [4] initially suggested that emission signals from the cutting process were of the burst type only. The reason for their conclusions could be due to the fact that burst signalsfrom chip entanglement and breakage were not separated from, and thus overshadowed the continuous signals from the other sources. About the same time, Grabec and Leskovar [5] reported the presence of continuous signals. Later investigation confirmed the presence of both continuous and burst signals [8,9]. Other aspects that have been studied include tool breakage [13,16,17,19,21-24], chip form detection [15], and thermal cracking [18]. A more comprehensive

review is given in the appendix.

To gain a better understanding of the characteristics of AE signals generated during the cutting process, efforts were made earlier in the project to develop models that predict the spectra of the signals from some of the sources. A brief discussion of the preliminary models developed follows.

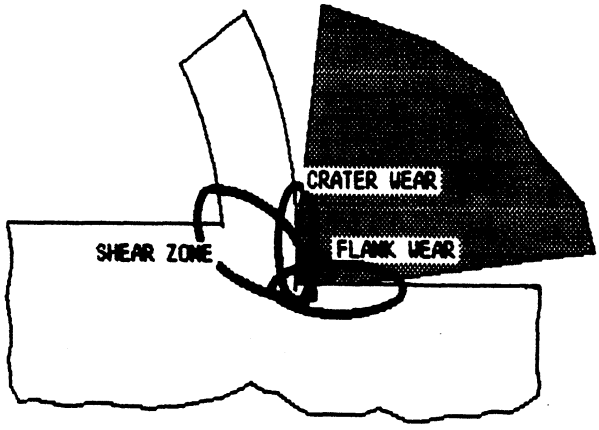

Figure 2. The zones of interest in the cutting process.

Preliminary Modeling of AE Source Mechanisms

SHEAR ZONE - The principle mechanisms responsible for separation of the chip from the parent material in the shear zone are plastic deformation (shearing) during continuous machining, or fracture during discontinuous machining. In the case of shearing, a fundamental model will have to consider the characteristics of AE generating during dislocation motion. However, since close examination of continuous chips often shows the chip to be formed by both microscopic deformation as well as macroscopic sliding of lamellae of material, the initial study involved an analysis of the frequency with which individual lamellae crossed the shear plane. This would give the macroscopic characteristics of AE from the shear zone.

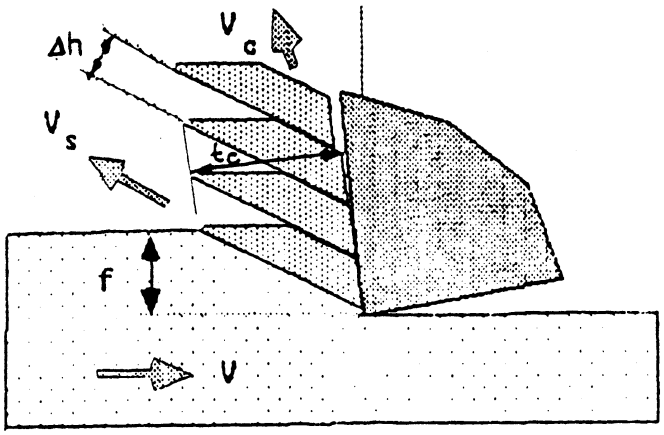

Figure 3. Formation of lamellae in the shear zone.

Using the configuration in Fig.3 [25], the frequency at which the lamellae cross the shear plane is given by:

$$f = \frac{V_c}{\Delta h} = \frac{r \cdot V}{\Delta h} \qquad (1)$$

where

V_c = chip velocity,
V = cutting velocity,
Δh = thickness of lamellar layers, and
r = chip thickness ratio.

Equation (1) indicates that the macroscopic contribution to the signal spectrum depends on the cutting conditions, and therefore a variation in cutting conditions, especially the cutting speed should be reflected in a shift in the frequency component due to macroscopic deformation.

The frequency values obtained from equation (1) will depend greatly on the values used for the lamellar layer thickness. Three possible alternatives are:

a. The thickness of the shear zone,
b. The thicknesses of deformed grains, in which case the lamellar sliding is attributed to grain boundary sliding, and
c. The separation distance between slip planes,

where each slip plane slides with respect to its neighbour as it crosses the shear plane. This is based on the assumption that the slip planes are oriented parallel to the shear planes. The interplanar distance, d, can then be calculated by the relation:

$$d = \frac{a}{\sqrt{h^2 + k^2 + l^2}} \qquad (2)$$

where

a = lattice constant for a cubic structure, and

h, k, l = Miller indices for the slip planes.

In addition to the macroscopic spectral components discussed above, there will be other spectral components that arise from the manner in which an individual dislocation releases energy. This aspect will be considered later.

SECONDARY AND TERTIARY ZONES - No models have been developed yet to predict the spectral characteristic of signals generated in these regions. However, it is expected that the microscopic contributions from individual dislocations will be the same as in the shear zone since bulk deformation occurs to some extent in the secondary and tertiary zones as well. On the macroscopic scale, the predominant wear mechanisms in each zone will need consideration. For example, if adhesive wear is considered predominant on the tool flank, then the rate at which individual asperity joints are formed and broken will be analysed in addition to the plastic deformation associated with each joint as well as fracture of the joint.

MACHINE TOOL VIBRATION - Vibration of the machine tool, even though not an acoustic emission source, does affect the detected signals since it is limited to the lower frequency ranges and AE transducers behave as accelerometers at low frequencies.

Consequently, it is necessary to identify the range of vibrational signals so that they can be filtered out. This would ordinarily require dynamic analysis of the machine tool structural modes. To simplify estimation of these frequencies, the analysis can be based on the waviness of the machine surface, and the dominant frequencies obtained from the relationship:

$$\frac{V}{\Delta S} \qquad (3)$$

where

ΔS = the wavelength of the waviness, (see Fig.4)

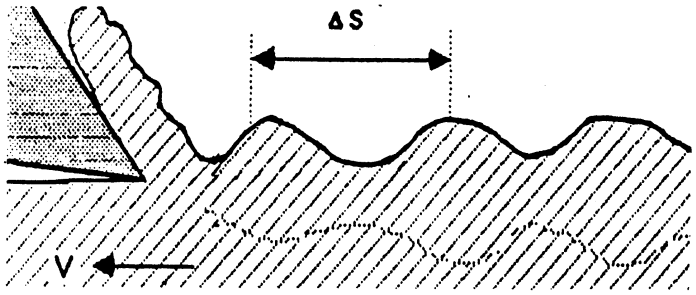

Figure 4. Surface waviness due to vibration

2.2 System Calibration

Acoustic Emission transducers of different makes always have different sensitivities. Even those of the same make from the same manufacturer do have significant differences in their sensitivities. Unfortunately, a number of manufacturers supply a single chart for all transducers of the same model which may not indicate their specific characteristics. Moreover, as a transducer is used, its characteristics may change with time. Finally the structure being monitored or the propagating medium does have an affect on the original signal. These explain the discrepancies that are sometimes reported between AE data obtained using apparently the same conditions but on different systems.

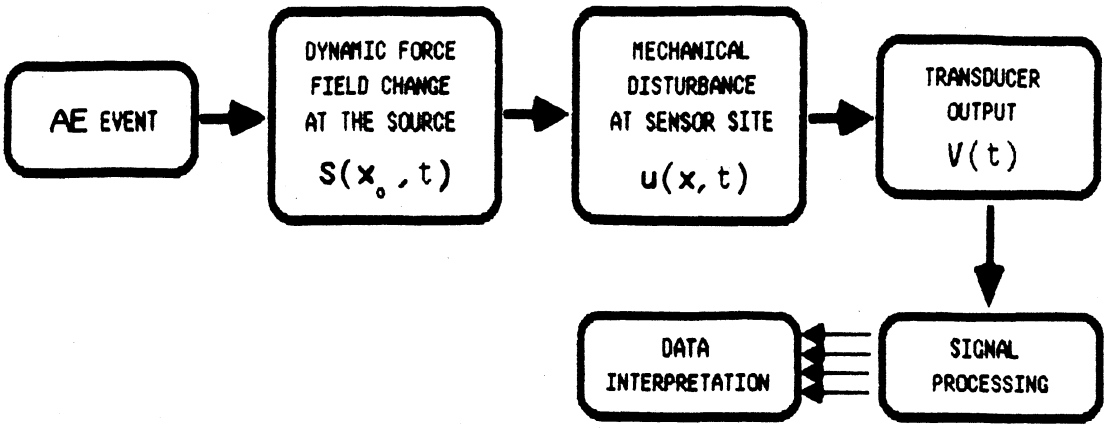

Figure 5a. AE source interpretation

Fig.5a explains the sequence of steps an AE event undergoes, from generation through detection and interpretation [26]. The event results in a stress wave or force tensor, $S(x_o, t)$ which propagates through the structure ,resulting in a displacement, $u(x,t)$, at the sensor site which is detected by the transducer. The modification to which the original signal is subjected by the propagating medium is given by its Green's tensor, $G(x, x_o, t-\tau)$, which represents the displacement in the structure at a point, x, and time, t, due to an impulse force applied at a point, x_o, and time, τ. The displacement at any point, $u(x,t)$, in the medium is then given by:

$$u(x,t) = \int_{-\infty}^{t} G(x, x_o, t-\tau) \cdot S(x_o, \tau) \cdot d\tau \qquad (4)$$

The output voltage of the transducer, $V(t)$, is a function of both the disturbance at its site $u(x,t)$, and the transfer function of the transducer. This is shown in block diagram form in Fig. 5b.

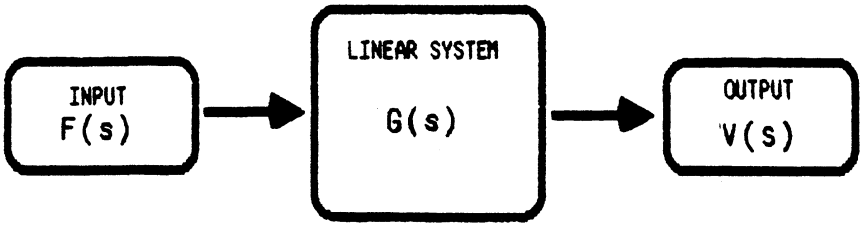

Figure 5b. Characterization of a linear system

The transfer function of the transducer can be obtained by applying an impulse source function to an infinite medium on which the transducer is mounted. A number of methods have been developed for simulating an impulse input, including breaking a glass capillary tube, a pencil lead and dropping a steel ball [26]. We have studied some of these methods, and another method which is considered more reliable is currently being developed.

The principal reason for developing a calibration method is to enable the characteristics of the propagating medium and instrumentation to be considered in analyzing AE signals, thereby eliminating or minimizing the problem of inconsistencies. The approach being used is based on the reciprocity concept, which is discussed next.

2.3 The Reciprocity Calibration Technique for Piezoelectric AE Transducers

Basic Equations

Transducer calibration is essential for quantitative evaluation of tool wear and breakage using AE and also for direct comparison of information obtained using different systems. If a relationship can be established between the input and output in an AE system, then by measuring the output voltage, it is possible to determine the characteristics of the source input.

As outlined in a previous progress report [24] , the reciprocity technique provides an absolute calibration. The method was originally developed for the calibration of microphones and speakers and was first applied to the calibration of piezoelectric AE transducers by Hatano and Mori [27].

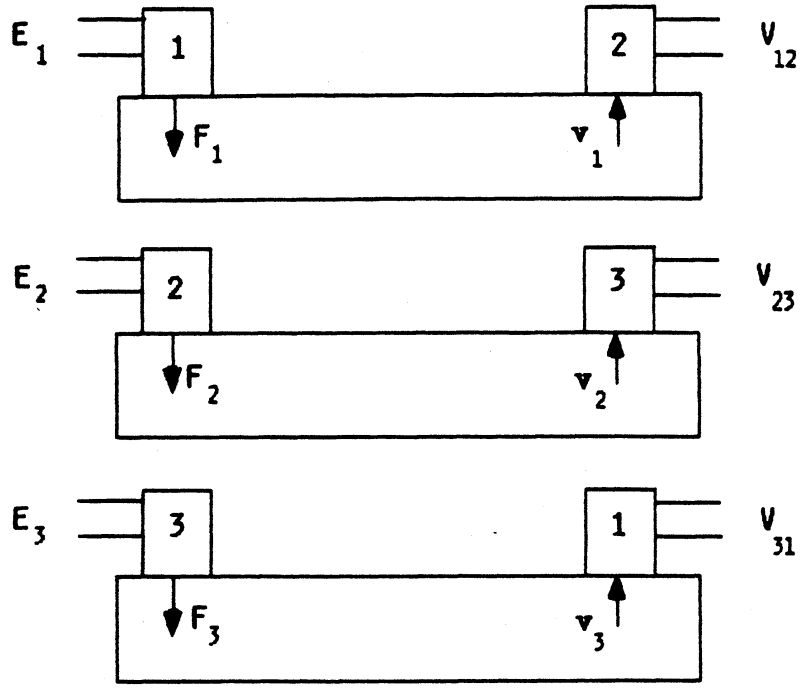

Fig. 6. Measurement setting of transducers

The method requires three reciprocal transducers which are used in sets of two as input and output devices, Fig. 6.

Three sets of measurements are done to find the calibration of each transducer. Measurements are made at a given frequency, f, and repeated in the range of interest, at given step increments. The basic equations required to calculate the transducer sensitivities are obtained as follows:

from Fig. 6, let

I : input current
E : input voltage
V : output open circuit voltage
Z : transducer impedance
v : vertical wave velocity

A reciprocity parameter, H, is defined as:

$$H = \frac{S}{M} \qquad (5)$$

Where S is the transmission voltage response, and M, the free field voltage sensitivity. M is defined as:

$$M = \frac{\text{Voltage across receiving transducer}}{\text{Vertical component of Rayleigh wave velocity at the receiver surface}} \qquad (6a)$$

and S is defined as:

$$S = \frac{\text{Vertical component of Rayleigh wave velocity at the receiver surface}}{\text{Input current at the transmitting transducer}} \qquad (6b)$$

For three reciprocal transducers, these become:

$$M_1 = \frac{V_{31}}{v_3} \qquad S_1 = \frac{v_1}{I_1}$$

$$M_2 = \frac{V_{12}}{v_1} \qquad S_2 = \frac{v_2}{I_2} \qquad (7)$$

$$M_3 = \frac{V_{23}}{v_2} \qquad S_3 = \frac{v_3}{I_3}$$

Using wave propagation theory, the reciprocity parameter is derived [27] as:

$$H = \frac{V_3}{F_3} = 2\pi f \cdot (1+\nu)/E \cdot k \cdot (2/\pi kD)^{1/2} \cdot X \qquad (8)$$

where,

$$k = 2.\pi.f.[2(1+\nu)\rho/E]^{1/2} .Y$$

D : distance between source and sensor
X,Y : constants obtained from Lamb's Equation
ρ : density of medium
ν : Poisson's ratio
μ : shear modulus
f : frequency of wave
F : input force
E : modulus of elasticity

The result is the same if H is defined for transducer 1 or 2. This parameter can now be used in equation (14) below to calculate

the transducer sensitivity.

From equations (7), we get:

$$V_{12} = M_2.v_1 = M_2\,(I_1.S_1) \quad (9)$$

$$V_{23} = M_3.v_2 = M_3\,(I_2.S_2) \quad (10)$$

$$V_{31} = M_1.v_3 = M_1\,(I_3.S_3) \quad (11)$$

Combining (9) and (10) gives:

$$\frac{V_{12}}{V_{23}} = \frac{M_2\,(I_1.S_1)}{M_3\,(I_2.S_2)} \quad (12)$$

If (12) is divided by (11),

$$\frac{V_{12}}{V_{23}\,V_{31}} = \frac{M_2}{M_3\,M_1} \cdot \frac{I_1}{I_2\,I_3} \cdot \frac{S_1}{S_2\,S_3} \quad (13)$$

Replacing all S in equation (13) by $S = H \,.\, M$, then the voltage sensitivity for the third transducer can be written as:

$$M_3 = \left\{ \frac{1}{H} \cdot \frac{I_1}{I_2\,I_3} \cdot \frac{V_{23}\,V_{31}}{V_{12}} \right\}^{1/2} \quad (14)$$

The current and voltage values in equation (14) are obtained experimentally and H is obtained from equation (8). M is calculated for each frequency in the range of interest to find the voltage sensitivity of transducer 3. The same procedure is repeated for other transducers. The units of M are volts per vertical wave velocity.

The voltage sensitivity can also be obtained by another approach. The calibration system modeling as signal transfer blocks in the frequency domain as shown in Fig.7 [28]. one then gets:

$$V_{12} = T_2 \cdot C_2 \cdot X \cdot C_1 \cdot T_1 \cdot I_1 \quad (15)$$

Similarly,

$$V_{23} = T_3 \cdot C_3 \cdot X \cdot C_2 \cdot T_2 \cdot I_2 \quad (16)$$

$$V_{31} = T_1 \cdot C_1 \cdot X \cdot C_3 \cdot T_3 \cdot I_3 \quad (17)$$

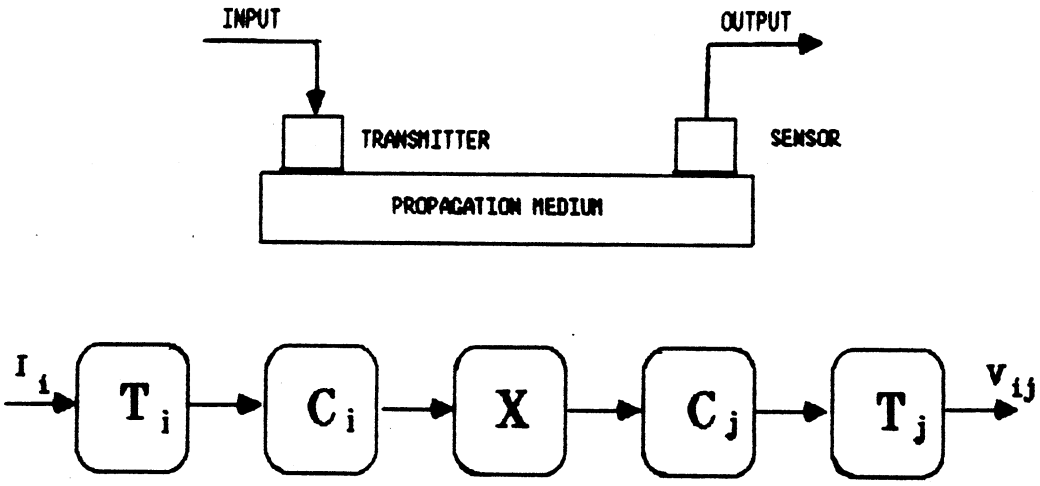

Figure 7. Transfer functions for reciprocity calibration

Equation (15),(16),(17) can be solved simultaneously to obtain:

$$C_3 \cdot T_3 = \left\{ \frac{1}{X} \cdot \frac{I_1}{I_2 I_3} \cdot \frac{V_{23} V_{31}}{V_{12}} \right\}^{1/2} \quad (18)$$

The transfer function of transducer 3 is given in equation (18), coupled to the couplant transfer function. For the derivation of equation (18), the transmitting and sensing transfer functions of a transducer is assumed to be equal. It can be observed that the transfer function approach yields the same results as equation (14) provided that $M_3 = C_3 \cdot T_3$ and $H = X$, which means the reciprocity parameter is equivalent to the transfer function of the propagating medium.

Limitation of Calibration

A number of investigators have used this technique and some AE transducer manufacturers are also calibrating their transducers by this technique [29]. The conventional approach is to use large

steel plates as propagating media and thus make use of Rayleigh wave theory for the transmission of the sinusoidal continuous signals.

Equation (8) was developed for infinite media and may not be directly applicable to structures of finite dimensions as a result of wave reflections in the medium. Furthermore, equation (8) depends greatly on the reciprocity of the transducers being used.

In equations (14) and (18), the input current values are used. It is assumed that this current value supplies the necessary energy to create pressure variations when the transmitting transducer is attached to the medium. Therefore the measurements of I, must represent the current which gives rise to the dissipation of energy.

To be able to apply this method to the calibration of transducers coupled to different structures, there is a need to obtain H or X by experimental methods. An approach to this problem will be discussed in the experimental section.

2.4 Signal Processing

A number of investigators have shown that the count, count rate, amplitude distribution, autocorrelation, and the RMS value of AE signals contain valuable information on the cutting process [4-10,22]. In general, these investigators studied the time domain features of signals. Unfortunately it is diffucult to incorporate the transducer characteristics in time domain analysis. Consequently, these previous investigations have had limited success. Our investigation is based on the frequency domain analysis and uses methodology similar to what has been applied in fields like speech recognition or video image processing [30] and have been highly succesful in these areas.

In the frequency domain, every AE signal generated by a different source is represented in a unique way. The AE sources in machining are basicaly located in the shear zone, flank and crater wear zones, as shown in Fig.2. The physical mechanisms in

each zone have been studied to some extent [8]. However, their relationship to AE are not fully established yet.

One aspect of this investigation has therefore involved a study of the spectral variation of AE from metal cutting during gradual tool wear, chip breaking and tool breakage. An effort was made to isolate each case, and AE signals were recorded. The power spectrum of these signals were then obtained on analog devices for visual observation. However as outlined in [31], visual observation is subject to eye fatigue, inconsistency, and subjective bias.

A technique that is currently under investigation is based on pattern recognition principles which eliminates human interaction by implementing the analysis in software. The first step in this direction will involve transformation of the digitized signal from the time domain to the frequency domain. Following transformation, the feature space (frequency domain) will be partitioned into regions that are characteristic of the various signal sources of interest. Such classification will require training of the system, for which prototype data for each of the signal sources will be used. With the boundaries of the various classes defined in the feature space, an incoming signal can be identified as to its source. For example, if a tool fractures during the cutting process, the overall nature of the signal will change, thus changing the spectrum (or position in feature space). Computing the position in the feature space, therefore, permits identification of the source of the detected signal.

The prototype data in the training set can be obtained in different ways. In metal cutting, these patterns correspond to different modes of tool wear, chip breaking, tool breakage or chip entanglement where each has different physical characteristics. It is considered that these differences are reflected in the AE signal frequency domain which can be identified as specific features [11]. The steps of signal analysis are shown in Fig. 8.

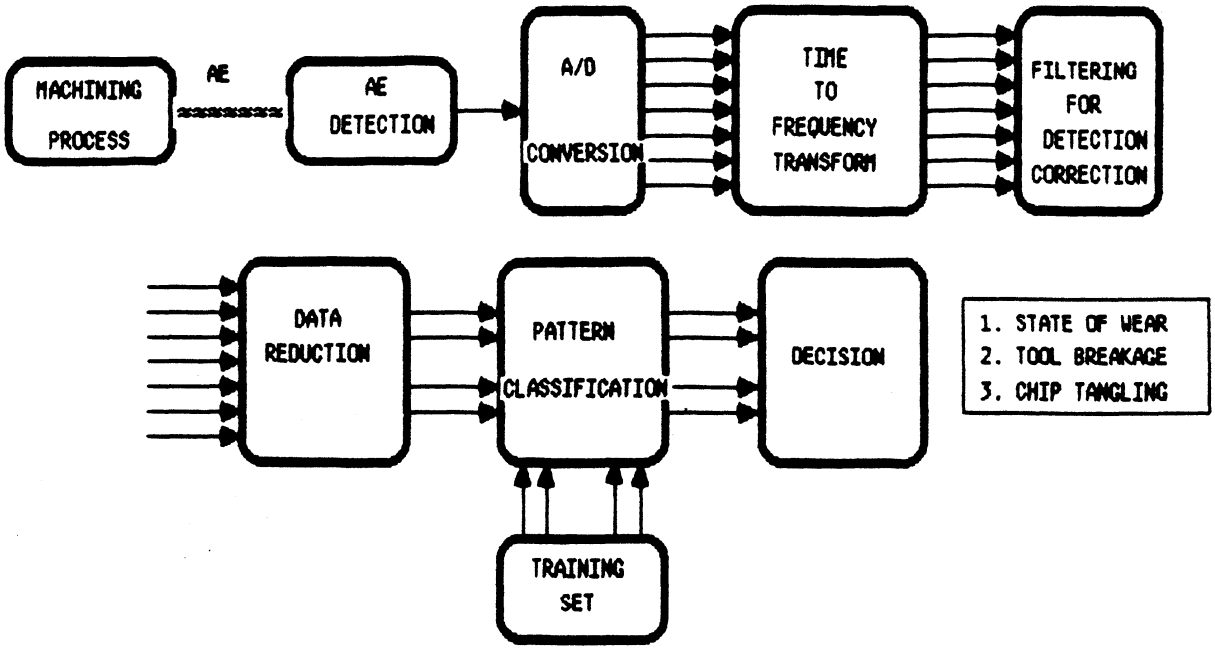

Figure 8. AE signal processing

3. EXPERIMENTS

3.1 Experiments on Metal Cutting

Preliminary machining experiments were undertaken to obtain a visual analysis of the power spectrum of AE signals recorded during the process. Various cutting conditions were used, and signals from both tool breakage and gradual tool wear monitored. The tests were conducted with the setup shown in Fig. 9. AISI 4140 steel and cast iron work materials were machined with carbide insert tools, and AE signals recorded using an AET FC500 piezoelectric transducer. Gradual wear measurements were obtained off-line with a tool maker's microscope. The various cutting conditions are listed in Table 1.

The AE signals were analyzed on a HP 8556 spectrum analyzer by

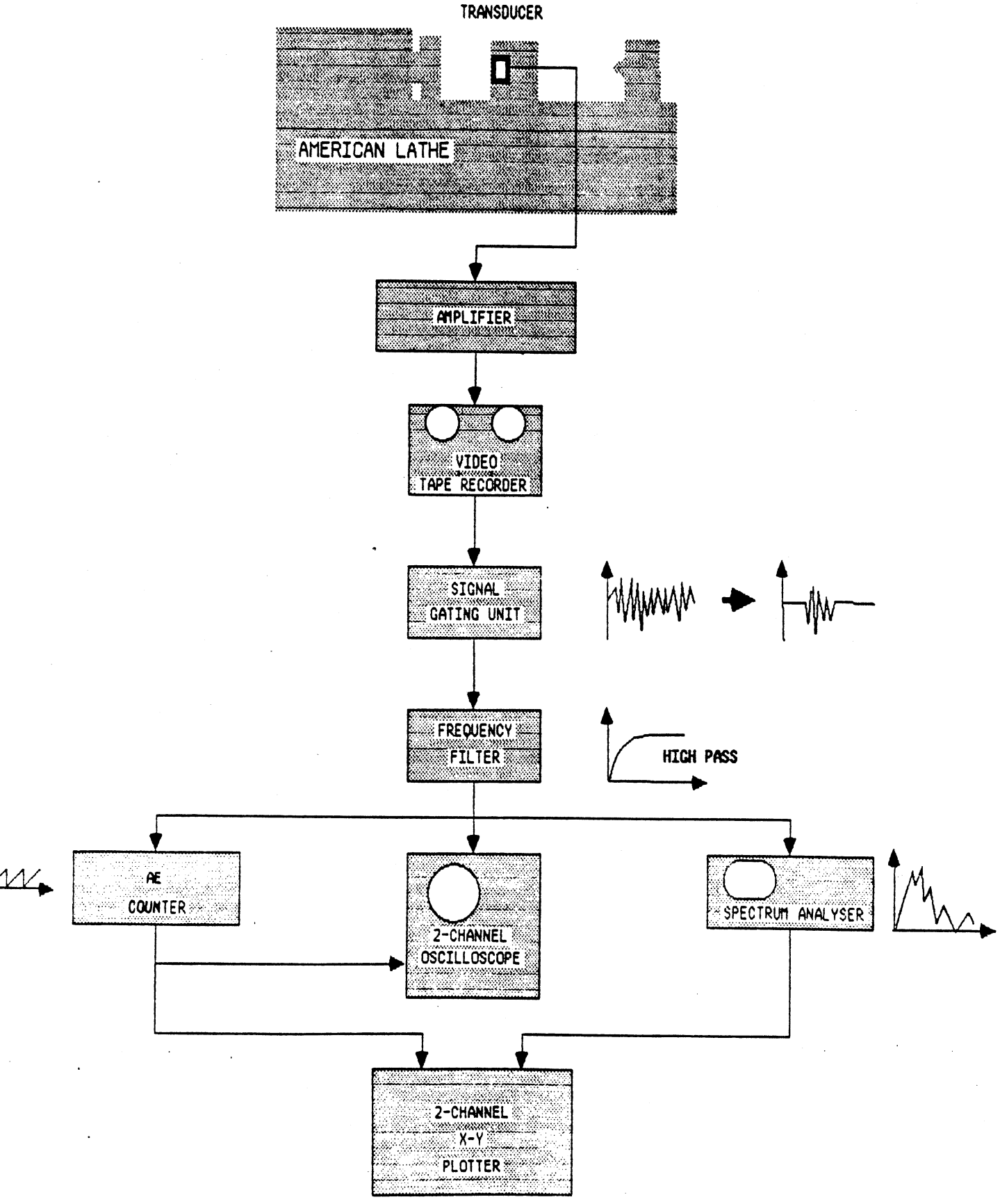

Figure 9. Experimental set-up for machining tests

playing back the previously recorded signals. The spectral analysis of Frequencies predicted by the source models were compared with the actual spectral peaks. Other experiments were done to investigate the frictionand wear effect by turning part materials and rubbing the cutting tool with different wear lands on the part without cutting. Count rate analyses were also done on the AET system. The results of these measurements and analyses will be discussed in section 4 of this report.

3.2 Experiments on System Calibration

Preliminary experiments on system calibration began with pencil lead breaking in our work. Using a tool holder and a 0.5 mm. pencil lead, impulse inputs were simulated by breaking the lead at various locations on the tool holder and sensed by the transducer at a fixed location. The spectrum of each waveform was obtained. By considering different input locations, the structural effects of the tool holder on AE waves were observed. The results of these measurements can be compared with the AE sectra from cutting tests to verify the resonant frequencies of the system.

Frequency characteristics of the AE source can be obtained approximately by subtracting the calibration values from the recorded spectra, provided that both spectra are logarithmically scaled. However, this is not a very accurate method. For a true calibration, numerical values of sensitivity are required.

3.3 Experimental Setup for Reciprocity Calibration

The computerized experimental setup was described in a previous report [24], and is shown schematically in Fig. 10 as part of the complete tool wear and breakage sensing system. Continued improvements on the test setup have been made and more accurate measurements were done after replacing the analog signal generator with a digital one. As a result, it is now possible to get very high frequency resolutions as well as accurate values of

frequencies.

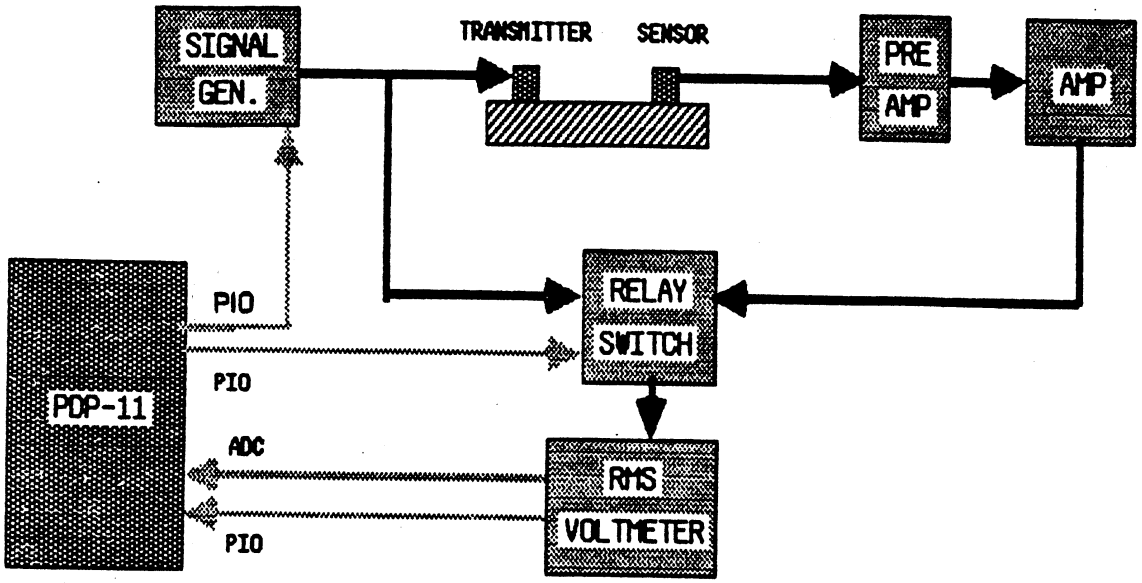

Figure 10. Calibration set up

3.3 Measurement of Input Current

The input currents in equations (10) and (14) can be simply measured using an ammeter. However, in the absence of such a device, the currents were calculated using measured voltage and transducer impedance values as described in a previous report [24]. Using the setup given in Fig. 11, the measurements for impedance calculation were done in the following order:

1. insert a carbon resistor, R,
2. set the sine wave generator to 1 MHz,
3. connect RMS voltmeter to measure E_R and set it to give 0 dB referenced to a 1 MHz input,
4. lower the frequency in the signal generator by small decrements until it gives -3dB reading,
5. get the respective frequency, f_c, at -3dB,

6. use

$$C_o = \frac{1}{2 \pi R f_c},$$

to obtain the capacitance value of the transducer and connection cables,

7. compute the transducer impedance from:

$$Z_f = \frac{1}{2 \pi f C_o}$$

at desired frequencies by changing f.

The pure capacitance of the transducers, however were obtained after subtracting the cable and connector contributions from the resultant value.

For R =84 kΩ, f_c =3348 Hz, C_c = 566 pf (cable and connectors)

R =45 kΩ, f_c =2122 Hz, C_T =1666 pf (total)

$$C_o = C_T - C_c = 1100 \text{ pf} \quad \text{for FC500}$$

and similarly for other transducers,

C_o = 500 pf for D9201
C_o = 500 pf for AET 375.

However, from the reciprocity calibration results, it is found that using a pure capacitor as a model of a piezoelectric transducer is not an exact representation. Consequently, modifications need to be made to the approach. As an alternative, the following method will be studied.

Hatano and Mori [28] proposed the use of a pure resistance inserted in series after the signal generator, and the voltage drop across R, E_R, to be measured, and subtracted from the voltage at the terminals of the generator, E, to find the voltage drop across the transducer. This is shown schematically in Fig. 11.

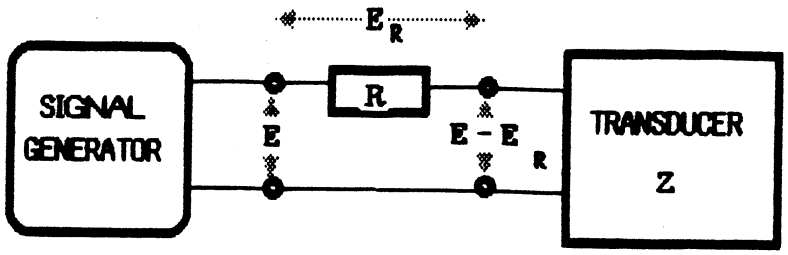

Figure 11. Voltage measurements for impedance calculation

In Fig. 11, since the same current is going through the resistance and the transducer, the impedance of the transducer, Z_f at a given frequency is calculated as:

$$Z_f = \frac{E - E_R}{E_R} \cdot R$$

By repeating this for every frequency in the range of interest, the impedance variation due to the frequency change can be obtained. During the actual calibration process, the current will be calculated from:

$$I = \frac{E}{Z_f} \quad .$$

3.5 Experiments for the Validity of Calibration

3.5.1 Propagating Medium

A cast iron measurement block with a polished surface is currently used as an infinite half space. Preliminary experiments were done to check the dispersive nature of the waves by simply observing the output signal from the calibration setup. For a given input sine wave, the effect of reflections would be an output signal, other than a pure sine wave.

Also, tool holder has also been used as the propagating medium. Whatever the characteristics of the propagating waves in

the tool holder structure, it is our goal to find the transfer function of the structure. As mentioned before, the reciprocity parameter, H, needs to be determined experimentally since the closed form was derived for infinite media.

Whatever the nature of waves in a structure, the vertical displacements are the inputs to a transducer. This is shown in Fig.13.

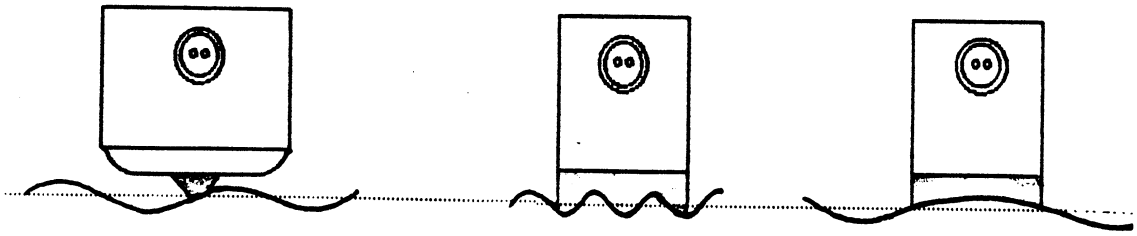

(a) (b) (c)

Figure 13. Sensing of surface displacements by various transducers

Using an infinite nondispersive structure, the characteristics of a transducer, M, can be obtained as in equation (14) or (18). Knowing M for all three transducers, a regular propagating medium such as a tool holder can be taken and the calibration procedure repeated for this medium. Having obtained M_i using an infinite half space medium, and measured I_i and V_{ij} for the tool holder set up, then the reciprocity parameter for the tool holder can be obtained from equation (14) as:

$$H = \frac{1}{(M_3)^2} \cdot \frac{I_1}{I_2 I_3} \cdot \frac{V_{23} V_{31}}{V_{12}} \qquad (14')$$

H, for the tool holder, can then be used as given in Fig.14.

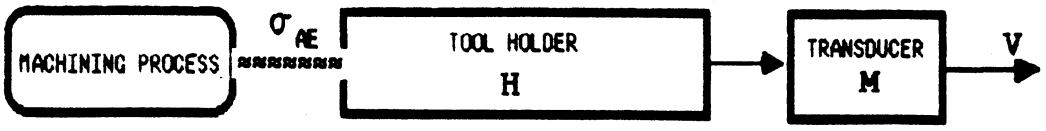

Figure 14. AE sensing during machining

Using the transfer block approach, the measured output V is given as:

$$V = \sigma_{AE} \cdot H \cdot M_3$$

σ_{AE} represents the input due to Acoustic Emission from the process. Measured output voltage is found from the product of the transfer functions of tool holder and transducer. Therefore using the above approach, the true characteristics of Acoustic Emission sources can be found by analyzing σ_{AE}.

3.5.2 Couplant

Currently, we use highly viscous liquid couplants to attach the transducers on to the structures . The couplant is used for better transmission of stress waves to the transducers. The effect of the layer thickness and of contact pressure have been studied experimentally. By applying different pressures on the transducer by using a clamp mechanism, the response of the transducer was obtained for various pressures.

Another factor of transducer sensitivity is the size effect. In Fig.13(a), a transducer with point contact wear plate is shown. In Figs.13(b) and (c), the effect of the size of the contact area is compared with high frequency and low frequency wave inputs. The high frequency wave is seen to have a cancelling effect due to the summation of displacements on the transducer surface which gives almost zero overall displacement in the steady state case. However in Fig.13(c), low frequency waves create sensible displacement. As

a consequence of this effect, the transducer in (b) becomes insensitive to the high frequency signals.

4. RESULTS AND DISCUSSION

Results obtained from the experiments in section 3 will now be presented and discussed.

4.1 Metal Cutting Tests

Preliminary experiments on metal cutting were listed in Table 1. The respective power spectra at selected wear states are shown in Fig.15a and b from above experiments. Also, given in Tables 2a and 2b, the predicted frequencies of signals from the shear zone, calculated from equation (1) using the test conditions.

TEST	V (FPM)	r	h (in)	f (KHz)
I-F	850	.54	.0045	20.3
II-F	675	.54	.0045	16.1
III-F	675	.65	.0060	14.6
IV-F	675	.84	.0040	28.4

Table 2a. Flank wear dominant tests

TEST	V (FPM)	r	h (in)	f (KHz)
I-C	400	.41	.0030	30.0
II-C	300	.41	.0030	40.0
III-C	300	.37	.0030	40.0
IV-C	400	.35	.0030	50.0

Table 2b. Crater wear dominant tests

It can be noticed that, there is some correspondence between the predicted frequencies and the spectral peaks as indicated by

arrows in Figs. 15a and b. However, there are other spectral peaks in the given ranges which are due to resonant frequencies of the sensing system. Thus, visual analysis of AE spectra becomes difficult unless the sensing system resonant peaks are filtered.

The frequency components due to machine tool vibrations were eliminated by filtering out frequencies below 20 KHz.

In addition to AE spectra plots, count rate plots were also obtained for the same machining tests. These are shown in Figs. 17a and b for the full period of experiments, and with intervals at indicated wear measurement points corresponding to those in Fig 15. The count rate measurements were not consistent with progressive wear due to difficulties in treshold setting of the counter. The results are discussed in greater detail in a previous progress report [23].

The AE spectra from friction tests of new and worn tools are shown in Figs. 16a and b for 200 and 800 fpm cutting speeds respectively. Distinct differences can be seen between the new and worn tools, and that is possibly due to the wear dependance of AE generation.

TEST NO	SPEED(fpm)	FEED(ipr)	DEPTH (in)	MAT'L	TOOL	FLANK(in)	CRATER(in)	TIME(min)
FLANK WEAR								
I-F	850	.0042	.100	CAST IRON	SNG 434A	.010	.003	1.00
					350	.013	.004	2.00
						.018	.007	4.00
II-F	675	.0042	.100	CAST IRON	SNG 434A	.008	.003	1.00
					350	.011	.007	2.00
						.017	.008	4.00
III-F	675	.0104	.100	CAST IRON	SNG 434A	.008	.007	1.00
					350	.011	.013	2.00
						.018	.015	4.00
IV-F	675	.0042	.050	CAST IRON	SNG 434A	.007	.003	1.00
					350	.012	.008	2.00
						.018	.013	4.00
CRATER WEAR								
I-C	400	.0104	.050	4140 STEEL	SNG 432	.007	.065	1.00
					K68	.007	.070	2.00
						.012	.080	4.00
II-C	300	.0104	.050	4140 STEEL	SNG 432	.003	.075	1.00
					K68	.006	.080	2.00
						.009	.085	4.00
III-C	300	.0168	.050	4140 STEEL	SNG 432	.005	.090	1.00
					K68	.007	.095	2.00
						.011	.095	4.00
IV-C	400	.0104	.080	4140 STEEL	SNG 432	.006	.065	1.00
					K68	.010	.075	2.00
						.013	.088	4.00

TABLE 1.

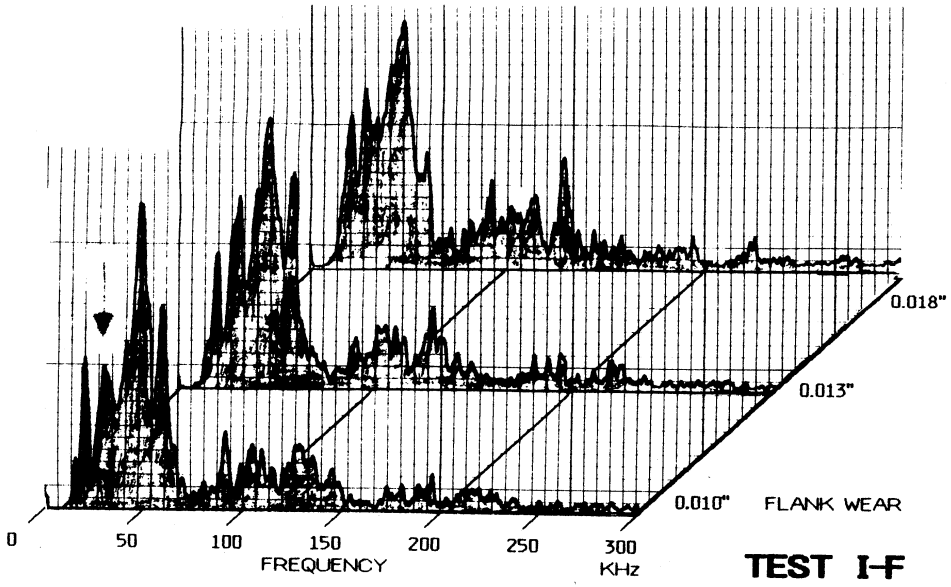
0.018"
0.013"
0.010"
FLANK WEAR
0
50
100
150
200
250
300
KHz
FREQUENCY
TEST I-F

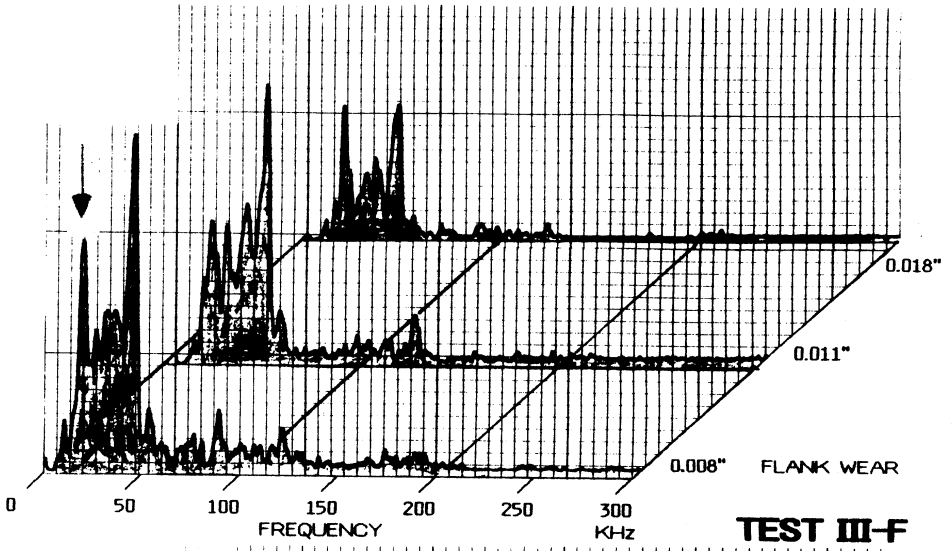
0.018"
0.011"
0.008"
FLANK WEAR
0
50
100
150
200
250
300
KHz
FREQUENCY
TEST III-F

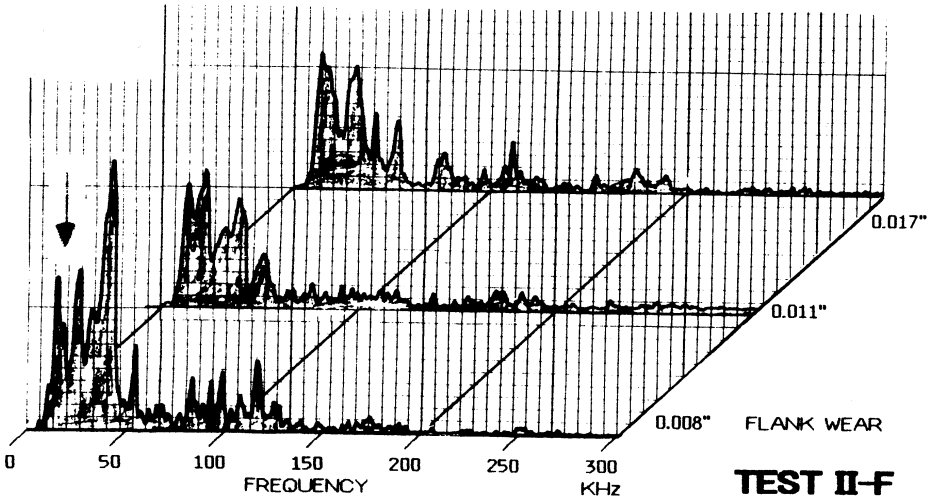
0.017"
0.011"
0.008"
FLANK WEAR
0
50
100
150
200
250
300
KHz
FREQUENCY
TEST II-F

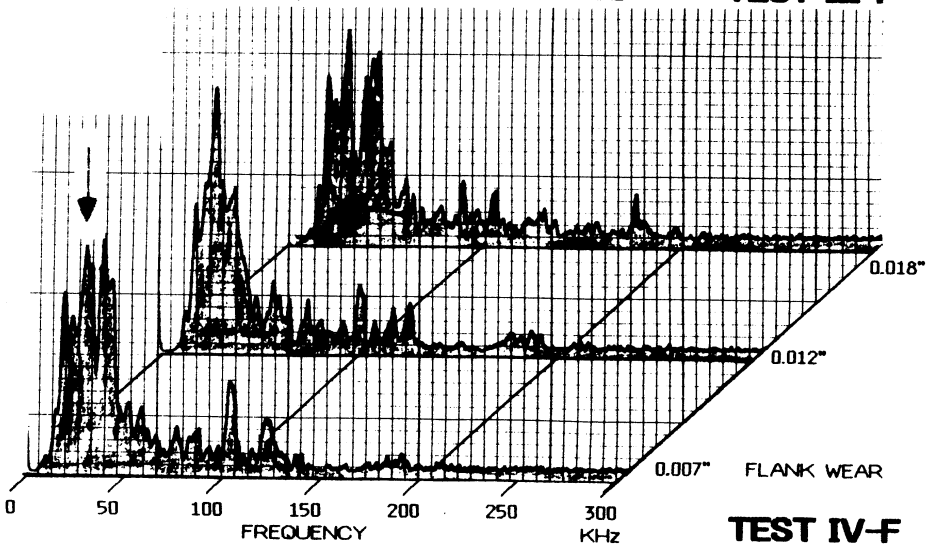
0.018"
0.012"
0.007"
FLANK WEAR
0
50
100
150
200
250
300
KHz
FREQUENCY
TEST IV-F

Figure 15.a

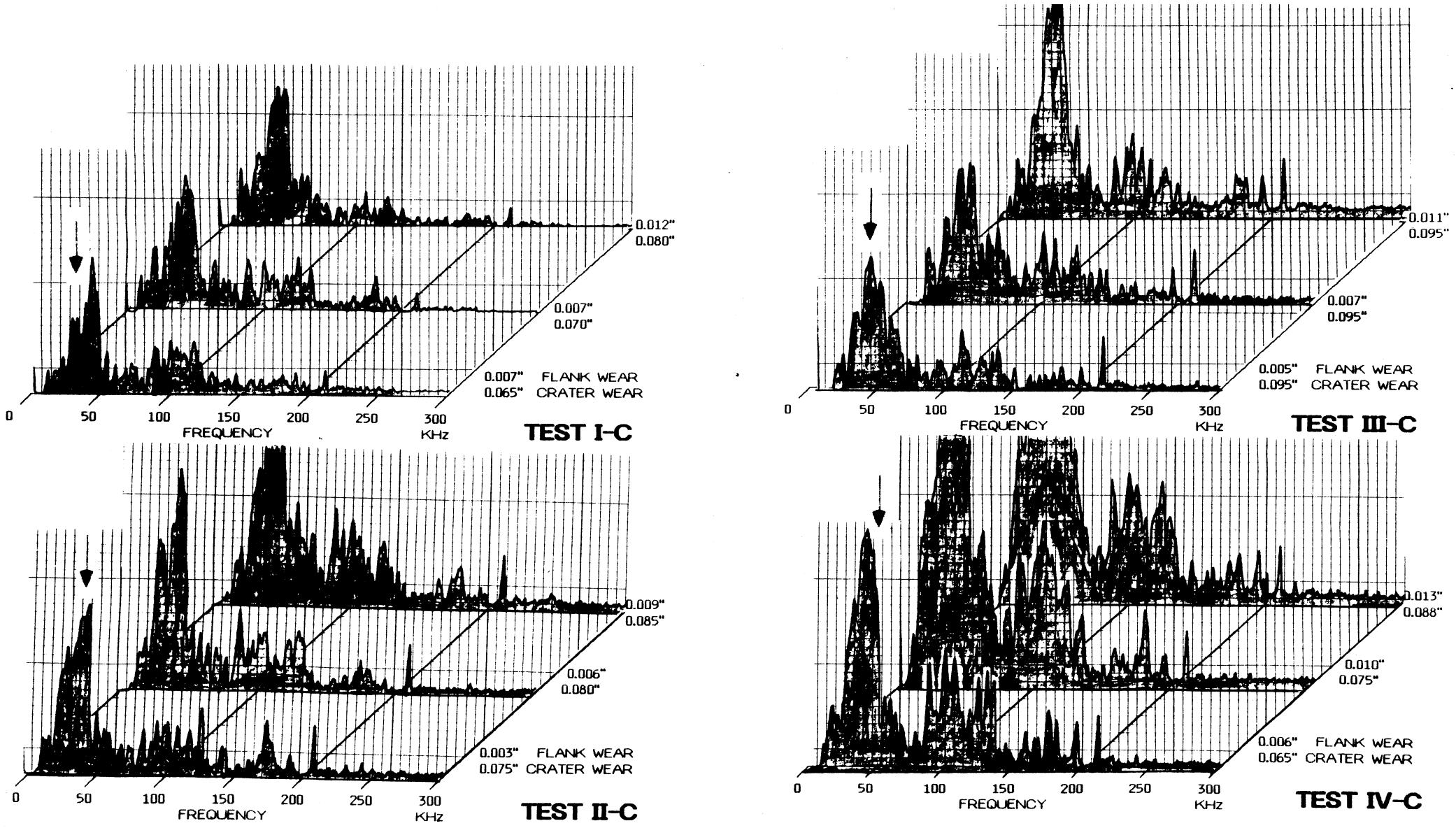
0.012"
0.080"
0.007"
0.070"
0.007" FLANK WEAR
0.065" CRATER WEAR
0
50
100
150
200
250
300
FREQUENCY
KHz
TEST I-C
0.009"
0.085"
0.006"
0.080"
0.003" FLANK WEAR
0.075" CRATER WEAR
TEST II-C
0.011"
0.095"
0.007"
0.095"
0.005" FLANK WEAR
0.095" CRATER WEAR
TEST III-C
0.013"
0.088"
0.010"
0.075"
0.006" FLANK WEAR
0.065" CRATER WEAR
TEST IV-C

Figure 15.b

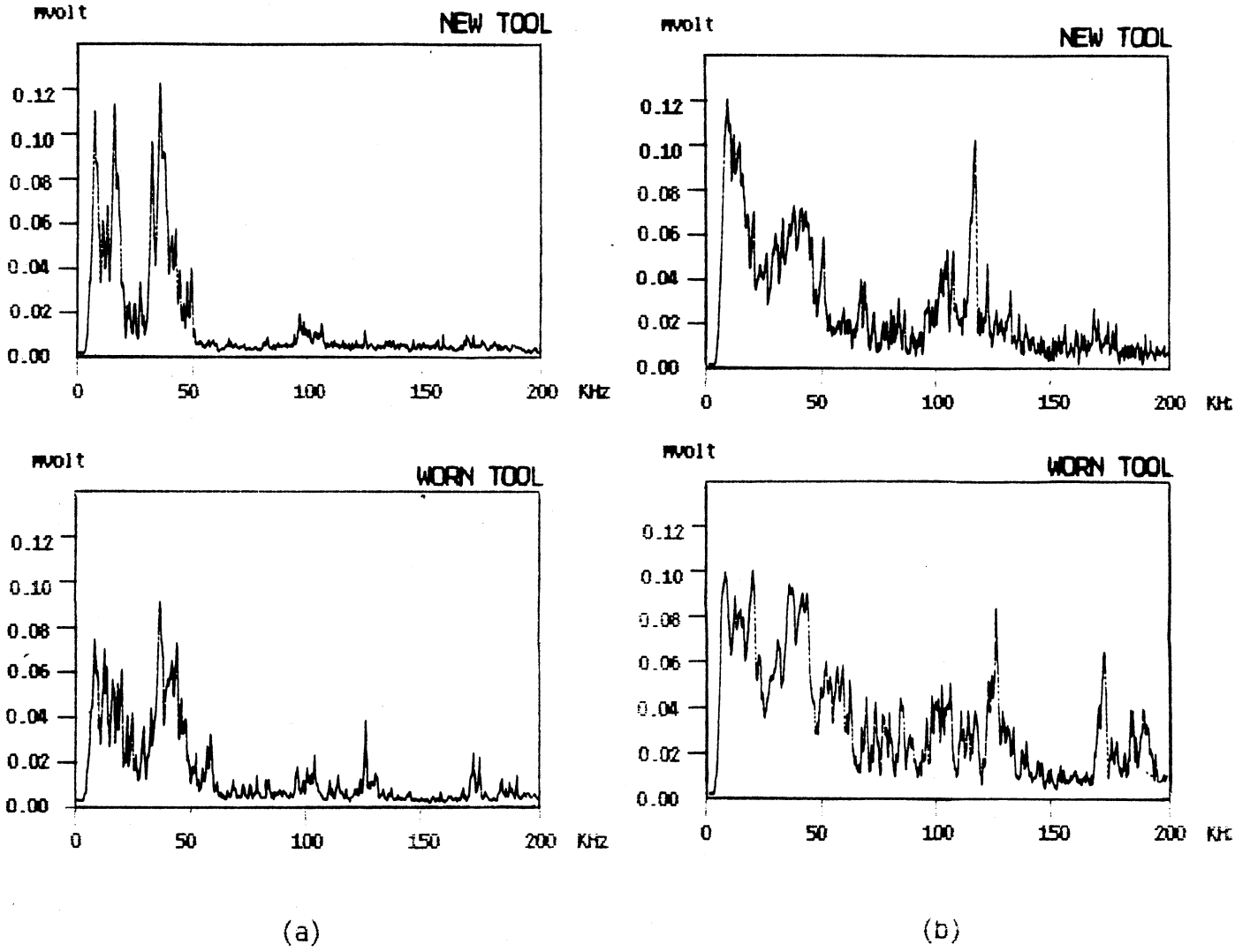

Figure 16 . Isolated friction and wear tests

a . V = 200 fpm, f = 0.0042 ipr,
carbide tool/cast iron part

b . V = 800 fpm, f = 0.0042 ipr,
carbide tool/cast iron part

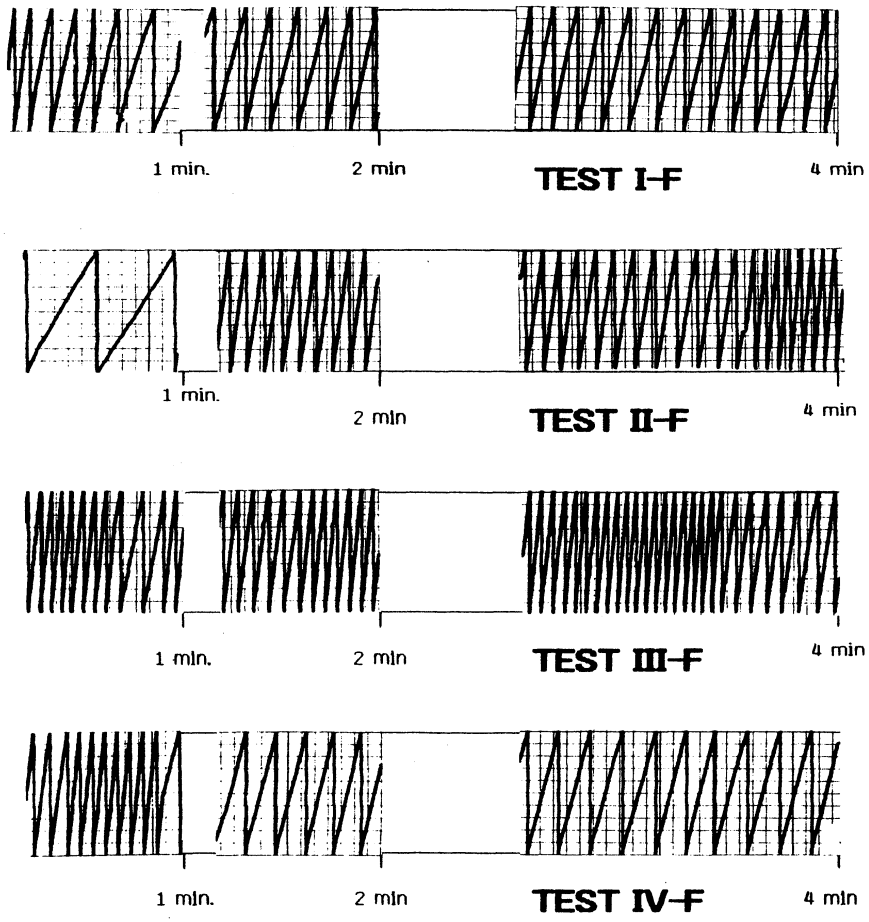

Figure 17.a AE count rates from flank wear dominant tests

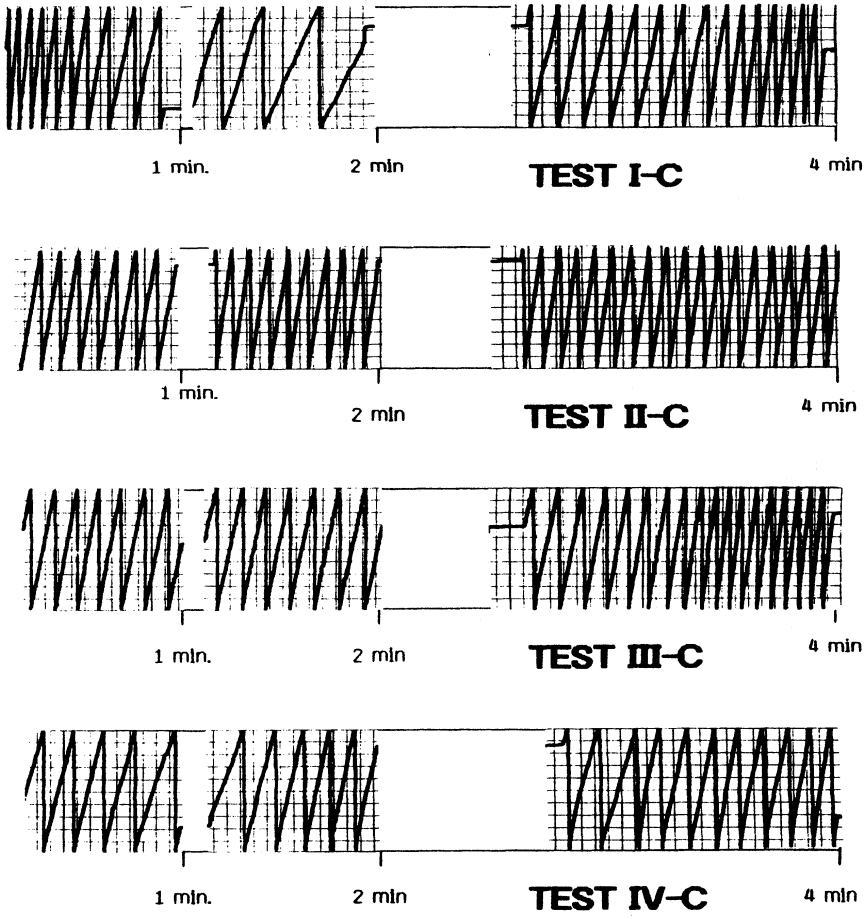

Figure 17.b AE count rates from crater wear dominant tests

4.2 Impulse Calibration Tests

In Figs. 18a, b, c, three pencil lead breaking responses of the AE sensing system (AET transducer FC 500) are shown, illustrating the effect of input location. Depending on the tool holder structure, the point where the lead is broken will change the $u(x,t)$, in equation (4), because the input function, $S(x_0,t)$, depends on the relative coordinates, x, of the source. The system resonances are seen to be concentrated around 50 and 100 KHz. In Fig 19, the frequency band of the spectrum in Fig. 18a is extended to 1 MHz.

Fig. 19 can be compared with Figs. 20a,b and c where AE spectra from metal cutting tests are shown. Fig. 20a is the spectrum of a tool breakage. Figs. 20b and c differ only by the cutting speed. After the spectral values of Figs. 20a, and b are divided by the ones in Fig. 19, the resultant spectral values show that the effect of cutting speed on AE generation is to raise the magnitudes of higher frequencies at higher speeds. However, these results lack the accuracy which is due to visual analysis of analog instrumentation. In the next section by using digital instrumentation, more accurate calibration values will be given, using the reciprocity calibration technique.

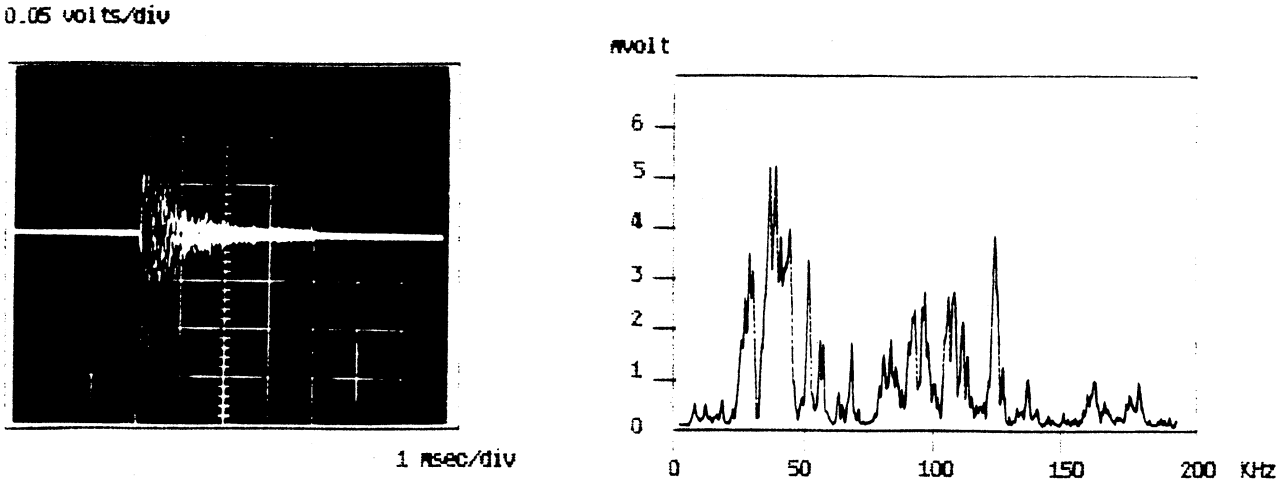

(a) TOOL SITE

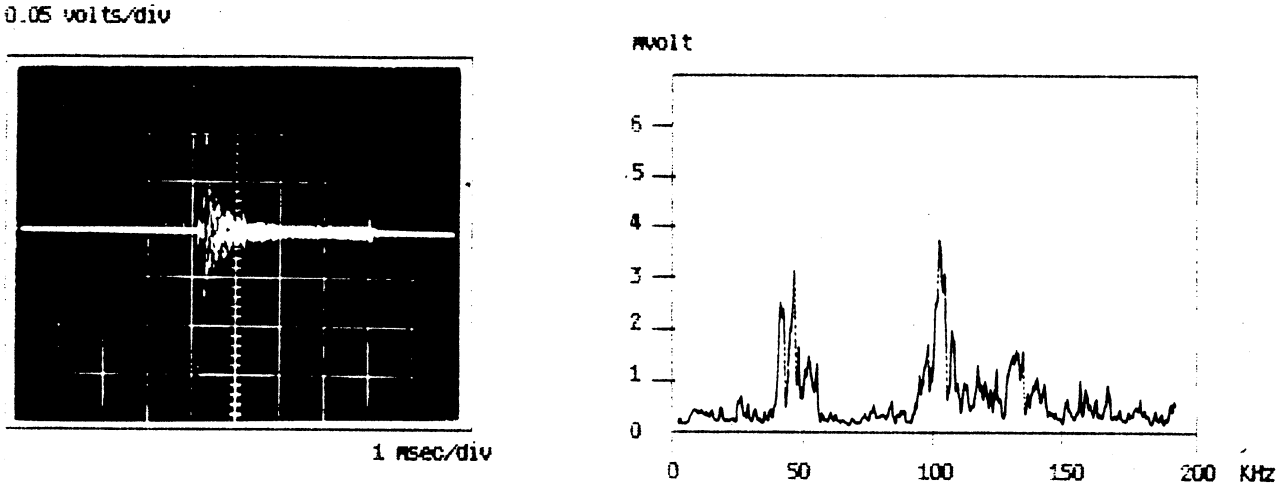

(b) MIDSPAN OF TOOLHOLDER

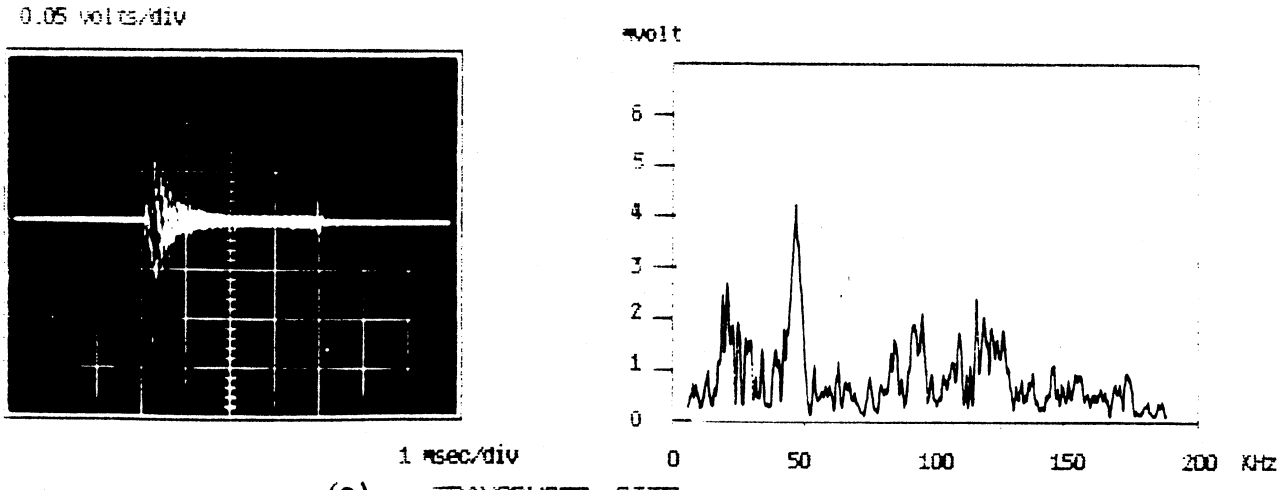

(c) TRANSDUCER SITE

Fig. 18 Time and Frequency Response of Transducer (FC 500) to an Impulse imput (breaking of pencil lead)

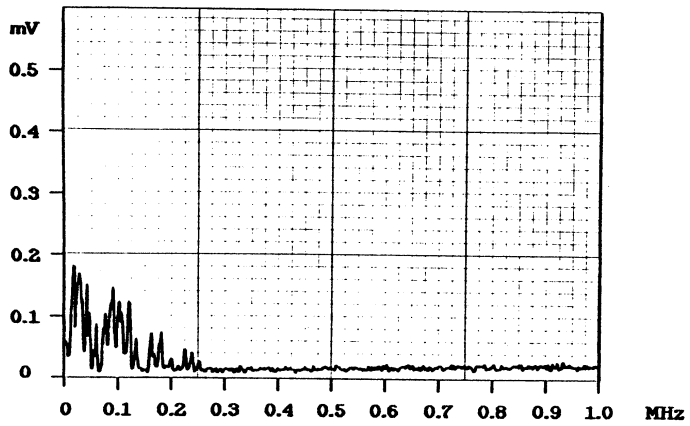

Figure 19. Frequency response for an impulse input (Amp. gain = 20 dB)

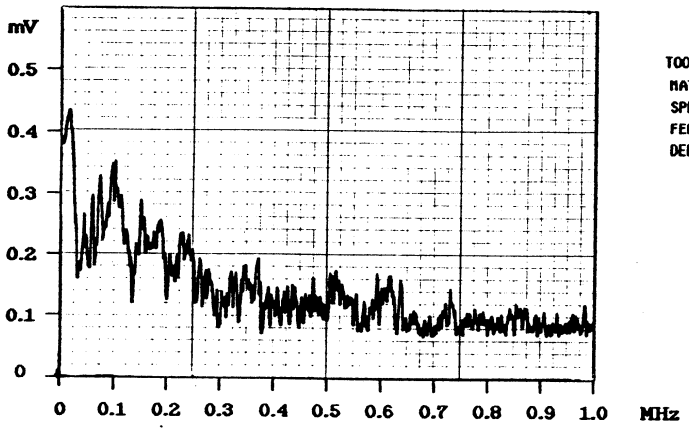

Figure 20.a Spectrum of AE from tool breakage (Amp. gain = 6 dB)

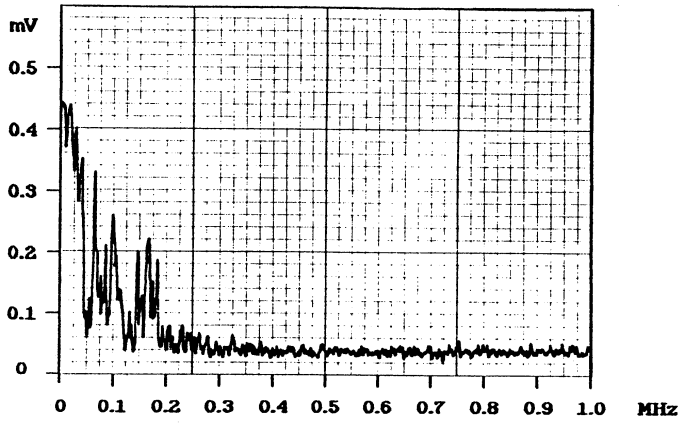

Figure 20.b AE spectra for : (Amp. gain = 19)

Cutting speed	=	675 fpm
Feed	=	0.0042 ipr
Depth	=	0.100 in
Material	=	cast iron
Tool	=	Carbide Al203 coated 350

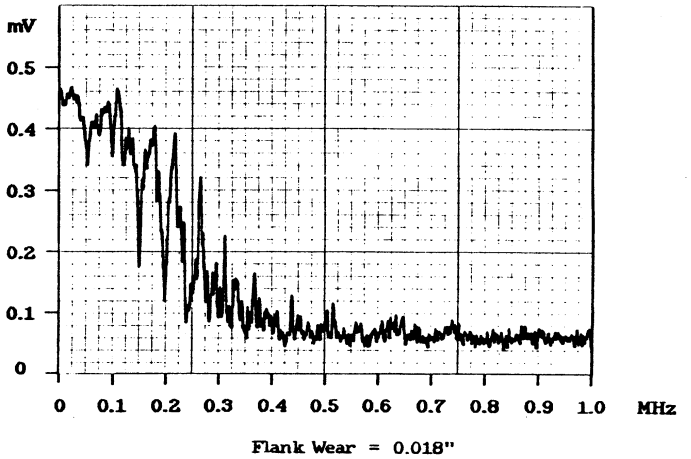

Figure 20.c AE spectra for : (Amp. gain = 15)

Cutting speed	=	850 fpm
Feed	=	0.0042 ipr
Depth	=	0.100 in
Material	=	cast iron
Tool	=	Carbide Al203 coated 350

4.3 Reciprocity Calibration Tests

The reciprocity calibration setup is shown in Fig. 10, and described in a previous report [24]. The previous version has been improved by using a digital signal generator. However some sources of error still needs to be eliminated. A modified RMS voltmeter is being used for voltage measurements, and the voltage readings are digitized using a 12-bit A/D converter in the computer. Thus, some inaccuracy is introduced through digitization.

Another error source is the energy bandwidth of an input signal. During calibration for given frequency increments, the energy band should have at least the same width as the increments. However, with the current set up, only a point frequency is used as illustrated in Fig.21.

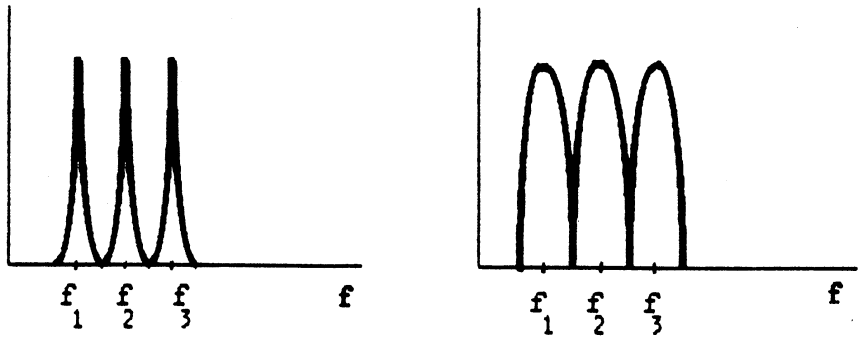

Figure 21. Energy band at each calibration frequency

The calibration was done for three transducers. Originally, the transducers were paired as follows:

1 - 2
2 - 3
3 - 1 .

The above ordering requires 3 reciprocal transducers. However, by using the following order, only one transducer is required to be

reciprocal.

1 - 2

1 - 3

3 - 2

The equations were modified in both cases and calibration charts obtained for the three transducers in either case and the results are presented in Figs. 22a, b, and c. Other than some gain variations, the location of peak values were found to be the same in both cases. Thus all three transducers can be considered to be reciprocal.

The calibrations were also repeated for a given setup to verify their repeatablity. The results are not presented. However, it was found that if calibrations are repeated without relocating the transducers, they are very repeatable. If transducers are removed and than reattached, and if exactly the same locations are not obtained , then the response varies. This can be explained by the combined effects of couplant thickness, directional sensitivity of the transducers, and the propagating medium transfer function. Predominant is the medium transfer function which is highly dependent on the spatial coordinates of the transducer locations.

The effect of couplant thickness was studied by attaching two transducers face to face and calibrating with different contact pressures. The pressure in effect varies the couplant thickness. The results of comparison of calibrations with full and no pressure are given in Fig.23. By using equation (18), the curves are obtained as the ratio of:

$$\frac{C_i \cdot T_i}{C^\circ_i \cdot T_i^\circ} ,$$

where $C_i \cdot T_i$, and $C^\circ_i \cdot T_i^\circ$ are the coupled transfer functions of the ith transducer under full pressure and no pressure cases respectively. It is assumed that $T_i = T_i^\circ$, and therefore the ratio represents the variation in the transfer function of the couplant.

The ratios of the coupled transfer functions of the transducer

and couplant are around 0 dB. Thus the contact pressure does not have a significant effect on the system response since the ratio of the full pressure and no pressure calibrations is about equal to unity.

In Fig.24, the calibration of a transducer with a small spherical contact point, the Brüel & Kjær type 8312, is shown. Those in Fig. 22 are regular AE transducers with large contact faces. The high attenuation in higher frequencies in cases of Fig. 22 are obvious. However, in Fig. 24, the point contact type sensor is highly sensitive to high frequencies.

Overall, the calibration curves obtained in our setup are very close to those provided by the manufacturers. The discrepencies are due mainly to the variations in calibration media. When these calibrations are compared with AE spectra of cutting tests in Fig.20, it has to be realized that the transducer used in cutting tests and in pencil lead breaking tests was the FC500, Fig. 22a. Also Fig. 22a is given in a logarithmic scale, whereas Figs. 20a, b are linear.

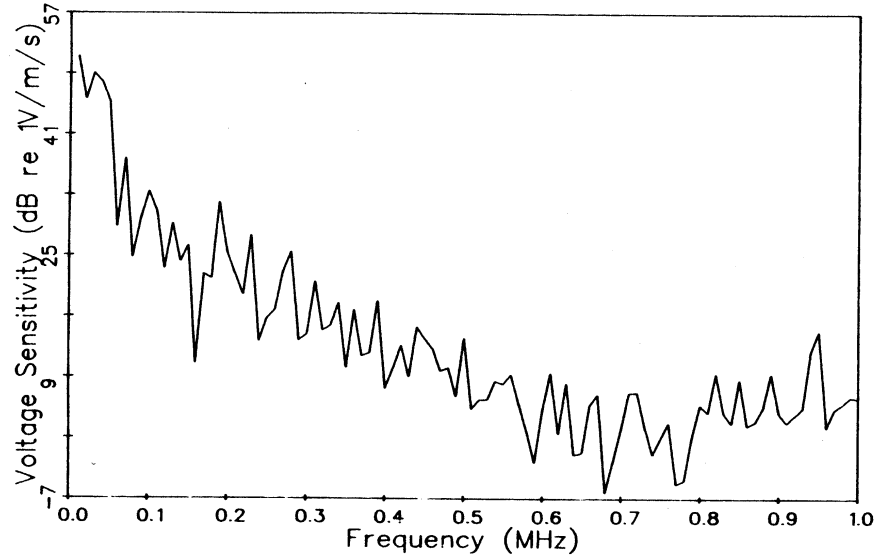

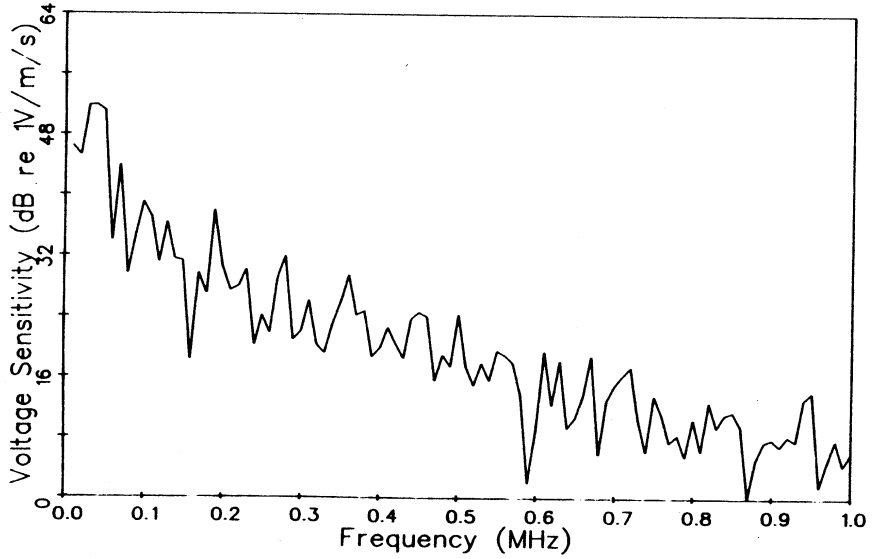

(a)

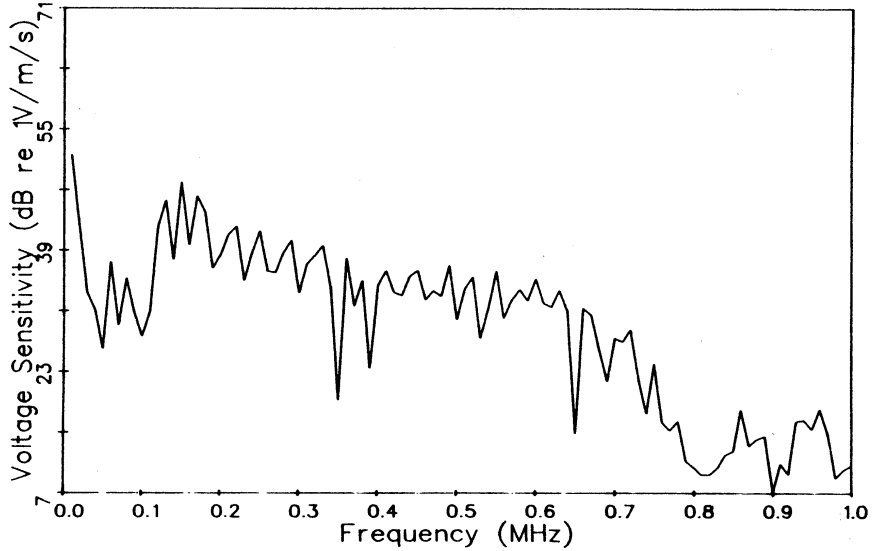

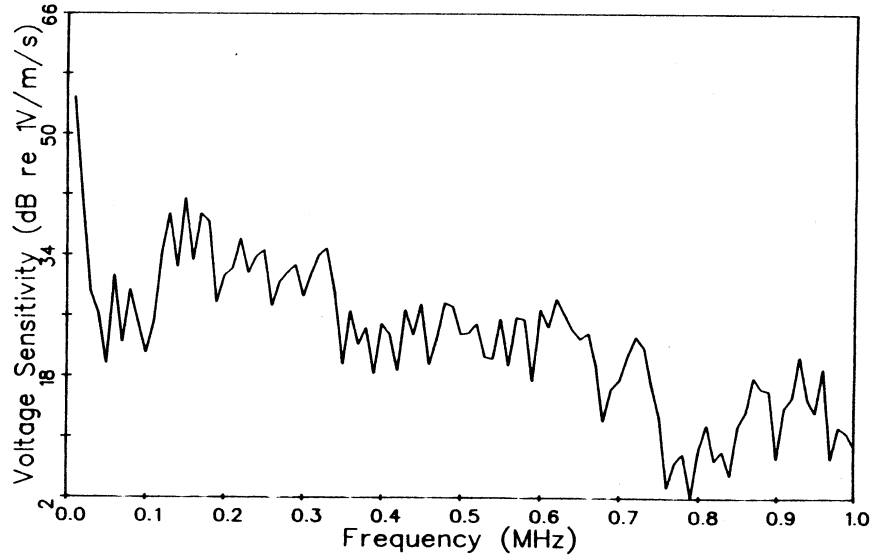

(b)

Figure 22. Reciprocity calibration of transducers:
(a) FC500, (b) D9201, (c) AET 375.
Upper curves from measurement set : (1-2),(2-3),(3-1)
Lower curves from measurement set : (1-2),(1-3),(3-2)

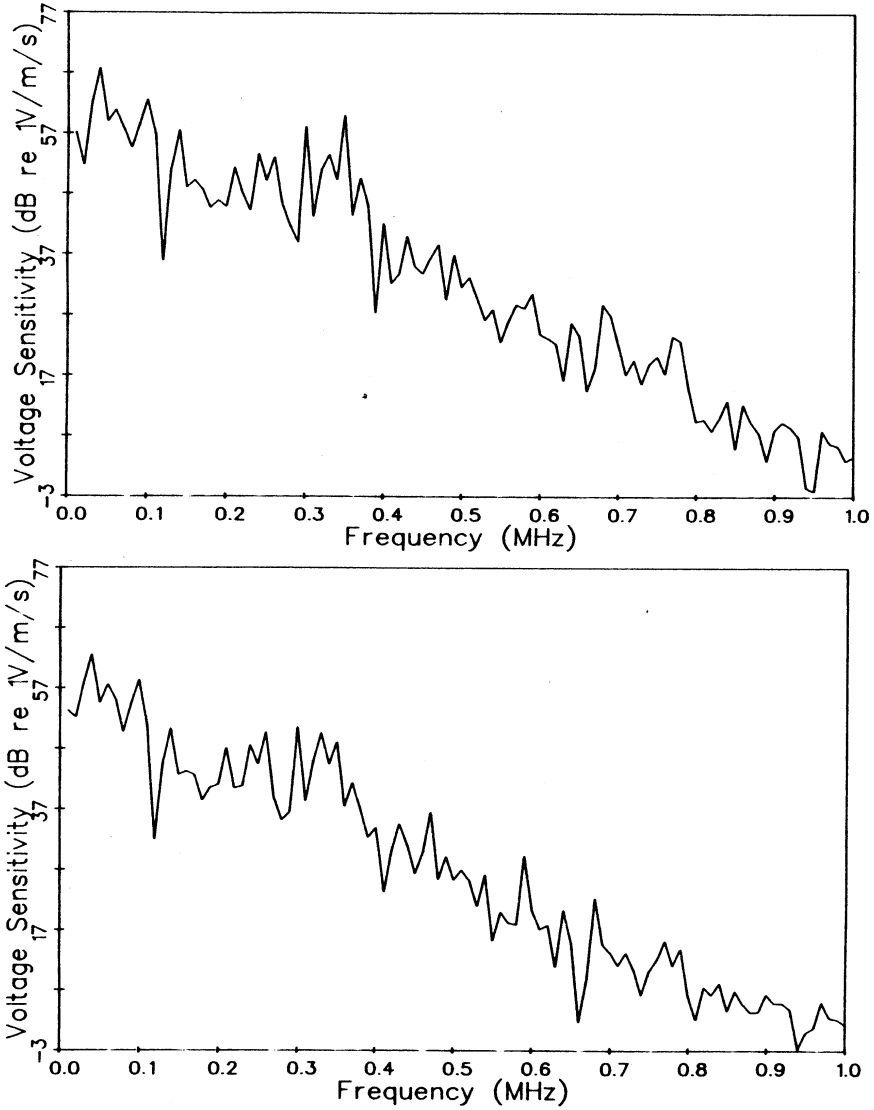
Voltage Sensitivity (dB re 1V/m/s)
77
57
37
17
-3
0.0
0.1
0.2
0.3
0.4
0.5
0.6
0.7
0.8
0.9
1.0
Frequency (MHz)
Voltage Sensitivity (dB re 1V/m/s)
77
57
37
17
-3
0.0
0.1
0.2
0.3
0.4
0.5
0.6
0.7
0.8
0.9
1.0
Frequency (MHz)

Figure 22.c

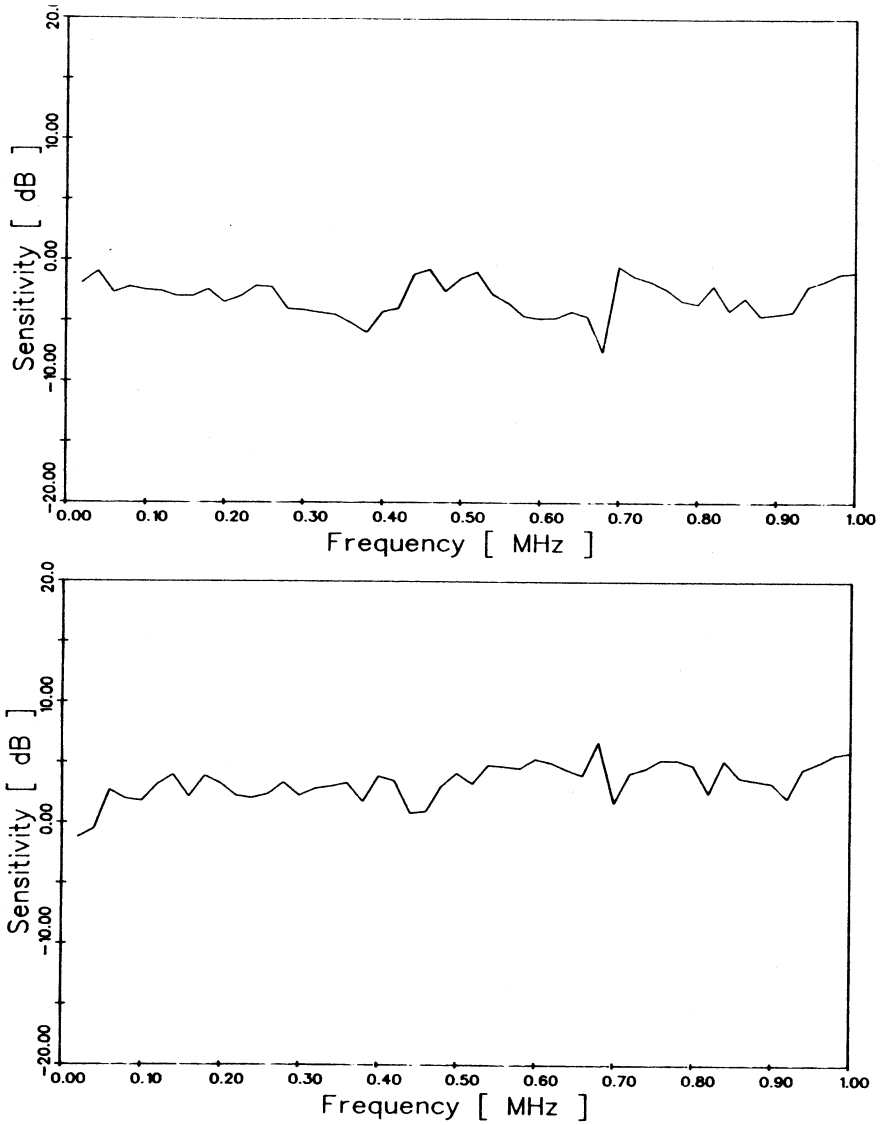

Figure 23. Pressure sensitivity of trasducers $(C \bullet T)/(C^{\circ} \bullet T^{\circ})$,
upper curve : FC500,
lower curve : D9201.

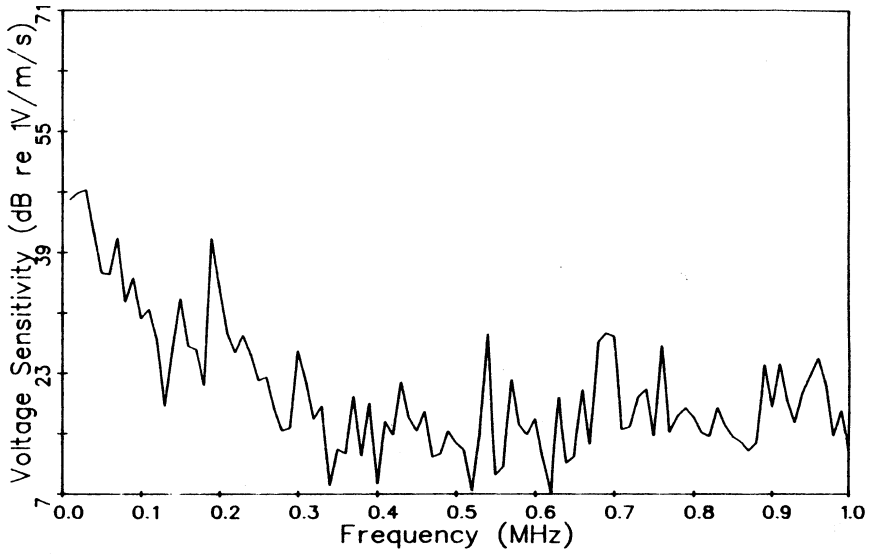

Figure 24. Reciprocity calibration of transducer Brüel & Kjær 8312.

5. CONCLUSIONS

The feasibility of using AE for tool wear and tool breakage monitoring during metal cutting has been studied and some experimental results are given in previous reports. It is found that AE signals, when analyzed from their frequency characteristics, give valuable information on the state of the cutting process. However, it is also found that the extraction of this information is possible only after the elimination of distortions introduced by the instrumentation.

Thus the system calibration was considered a necessary step. Using the reciprocity calibration method, a computerized experimental setup has been developed.

Recent work has focused on verification of the assumptions on which the reciprocity technique is based, as well as the effects of coupling and transducer size. The transducers used were found to have about the same characteristics when used either as a transmitter or sensor. This, however, will generally not be true of all transducers. It was also found that a variation of spatial coordinates of the transducer location referenced to the propagating structure had a strong influence on the results of calibration. Due to the standing waves, the surface of the structure has constant amplitude points which are minimum at the nodes of the waves. Therefore it is concluded that for a given calibration and actual sensing procedures, AE transducers have to be located exactly at the same point and with the same orientation.

The effect of the sensor size was also studied, and transducers with small aperture were found to be more sensitive to high frequencies and have relatively flat response. In conventional transducers, the aperture effect and also the design combinations create many resonant frequencies and low sensitivity at high frequencies. It might therefore be advantageous to use improved designs like the conical piezoelectric transducers.

From the results of the present work, it is concluded that a direct comparison of AE results obtained using different set-ups should generally not be made without taking into consideration, the characteristic effects of the instrumentation and propagating medium, both of which are likely to differ for various set-ups. The determination of the system characteristics hes been the recent focus of the project. The methodology developed is considered efficient, fast and reliable. One aspect that needs further consideration, however, is a more general determination of the reciprocity parameter.

The present phase of the investigation will form the basis towards identification of the sources of a detected signal, and their characteristics. Such an analysis will be the focus of subsequent work.

REFERENCES

[1] Cook. N. H., et al, "Survey of the State-of-the-Art of Tool Wear Sensing Techniques", MIT report prepared under NSF grant No.FI-43861, 1975.

[2] Micheletti, G. F., et al, "In-Process Tool Wear Sensors for Cutting Operations", Annals of the CIRP, Vol. 25, 1976, pp.483,496.

[3] Tlusty, D. J., and Andrews, G. C., "A Critical Review of Sensors for Unmanned Machining", Annals of the CIRP, Vol.32, 1983.

[4] Iwata, K. and Moriwaki, T., "An Application of Acoustic Emission Measurement to In-Process Sensing of Tool Wear ", Annals of the CIRP, Vol.26, No. 1, 1977, pp.21-26.

[5] Grabec, I., and Leskovar, P., "Acoustic Emission of a Cutting Process", Ultrasonics, Jan. 1977, pp.21-26.

[6] Dornfeld, D. A., "An Investigation of Orthogonal Cutting via Acoustic Emission Signal Analysis",Proceedings of the 7th North American Manufacturing Research Conference, The University of Michigan, Ann Arbor, MI, 1979, pp.270-274.

[7] Dornfeld, D. A. and Kannatey-Asibu, Jr., E.,"Acoustic Emission during Orthogonal Metal Cutting", Int. J. Mech. Sci., Vol. 22, No. 5, 1980, pp.285-296.

[8] Kannatey-Asibu, Jr., E.,"Investigation of the Metal Cutting Process Using Acoustic Emission Signal Analysis", Ph.D. Thesis, University of California, Berkeley, 1980.

[9] Kannatey-Asibu, Jr., E. and Dornfeld, D. A., "Quantitative Relationships for Acoustic Emission from Orthogonal Metal Cutting", Trans. ASME, J Eng. Ind., Vol.103, 1981, pp.330-340.

[10] Kannatey-Asibu, Jr., E. and Dornfeld, D. A., "A Study of Tool Wear Using Statistical Analysis of Metal Cutting Acoustic Emission", Wear, Vol.76, 1982, pp.247-261.

[11] Kannatey-Asibu, Jr., E., "On the Application of the Pattern Recognition Method to Manufacturing Process Monitoring", Proceedings of the 10th North American Manufacturing Research Conference, May 1982, pp. 487-492.

[12] Dornfeld, D. A., "Acoustic Emission and Metalworking-Survey of Potential and Examples of Applications",

Proc. of the 8th North American Metal Working Research Conference, University of Missouri - Rolla, 1980, pp.207-213.

[13] Moriwaki, T., "Detection for Cutting Tool Fracture by Acoustic Emission Measurement", Annals of the CIRP, Vol. 29, No.1, 1980, pp.35-40.

[14] Lan, M. S. and Dornfeld, D.A., "Experimental Studies of Tool Wear via Acoustic Emission Analysis", Proceedings of the 10th North American Manufacturing Research Conference, McMaster University, Hamilton, Ontario, May 1982, pp.305-311.

[15] Dornfeld, D.A. and Lan, M. S., "Chip Form Detection Using Acoustic Emission", Proc. 11th NAMRC, University of Wisconsin, Madison, Wisconsin, May 1983, pp.386-389.

[16] Kakino,Y.,"In-Process Detection of Tool Damage by Monitoring AE", Ame. Soc. for Metals, "Cutting tool materials", Proceedings of an Int. Conf., Sept.1980, pp.29-43.

[17] Inasaki, I. and Yonetsu, S., "In-Process Detection of Cutting Tool Damage by Acoustic Emission Measurement", Proc. 22nd MTDR Conference, 1981, pp.261-268.

[18] Kakino, Y., Suizu, H., Hashitai, M., Yamada, T., Yoshioka, H., and Fujiwara, A., "In-Process Detection of Thermal Crack of Cutting Tool by Making Use of Acoustic Emission", Bull. Japan Soc. of Prec. Engg., Vol.17, No.4, 1983, pp.241-246.

[19] Lan., M.S., and Dornfeld, D.A., "In-Process Tool Fracture Detection" Trans. ASME, J. Eng. Materials and Technology, Vol 106, Apr. 1984, pp.111-118.

[20] Uehara, K. and Kanda, Y., "Identification of Chip Formation Mechanism Through Acoustic Emission Measurements", Annals of the CIRP, Vol.33, No.1, 1984, pp.71-74.

[21] Ulsoy, A. G., and See, H. Y., "Tool Breakage Detection in Turning", Consortium Report, December 1983.

[22] Ulsoy, A.G. and Han, E., "Tool Breakage Detection in Turning Using a Multi-Sensor Strategy", Consortium Report, Dec. 1984.

[23] Emel, E. and Kannatey-Asibu, Jr., E., "Acoustic Emission Sensing of Wear and Tool Treakage- Signal Classification-", Consortium Report, Nov. 1983.

[24] Emel, E. and Kannatey-Asibu, Jr., E., "Acoustic Emission Transducer Calibration by Reciprocity Technique", Consortium Report , No.84-8, Sept.1984.

[25] Merchant, M. E. "Mechanics of the Metal Cutting

Process", J. Appl. Phy., Vol.16, No.5, 1945, pp.267-275.

[26] Hsu, N. N., and Breckenridge, F. R., "Characterization and Calibration of Acoustic Emission Sensors", Materials Evaluation, Vol.39, No.1, 1979, pp.60-68.

[27] Hatano, H. and Mori, E., "Acoustic Emission Transducer and its Absolute Calibration", J. Acoust. Soc. Am. , Vol.59, No.2, Feb.1976, pp.344-349.

[28] Hill, R. and Adams, N.L., "Reinterpretation of the Reciprocity Theorem for the Calibration of Acoustic Emission Transducer Operating on a Solid", Acoustica , Vol. 43, 1979, pp.305-312.

[29] Product Data, Brüel & Kjær Instruments, Inc., Marborough, MA.

[30] Ahmed,N. and Rao, K.R., Orthogonal Transforms for Digital Signal Processing, Springer-Verlag, New York, 1975.

[31] "Algorithms Could Automate Cancer Diagnosis", NASA Tech. Briefs, Technical Support Package, Vol.6, No.1, Spring 1981. Work done by Amyar A. Bady and Don Q. Winkler.

APPENDIX A

ACOUSTIC EMISSION MONITORING OF THE METAL CUTTING PROCESS

-A REVIEW

Among the earliest studies on AE monitoring of the cutting process were the works of Iwata and Moriwaki [4]; Grabec and Leskovar [5]; and Dornfeld and Kannatey-Asibu [6-12]. Iwata and Moriwaki [4] initially suggested that emission signals from the cutting process were of the burst type only. The reason for their conclusion could be due to the fact that burst signals from chip entanglement and breakage were not separated from, and thus overshadowed the continuous signals from other sources. About the same time, Grabec and Leskovar [5] reported the presence of continuous signals. Later investigation confirmed the presence of both continuous and burst signals [8,9].

Iwata and Moriwaki [4] used transducers that were calibrated by the reciprocity technique to detect AE signals during a shaping operation, simultaneously from the tool side and workpiece side, and suggested that signals from the two locations were similar. They further observed that the signal amplitude was attenuated as the transducer was located farther away from the cutting zone. In addition, the frequency content of AE from machining was considered to be concentrated in the 0 to 400 KHz range, and the influence of the chips was found to be significant. By measuring AE during idle running of a lathe machine, it was deduced that AE was hardly affected by ambient vibrations and noise.

In relation to the signal analysis, no significant changes in the signal spectrum was observed as flank wear progressed, a factor that can be attributed to problems associated with visual observation of a spectrum analyzer output. The RMS voltage and power spectrum, however, increased with wear initially, and then saturated. The count was also found to be negligibly small for low wear values, and then increased with wear either linearly or quadratically, depending on the threshold voltage. Plain carbon 1045 steel workpiece and carbide P10 cutting tools were used for the turning tests. Subsequent studies by the same group involved machining plain and alloy carbon steels using both carbide and ceramic tools. This time, the count rate was found to saturate after extensive wear.

Investigations by Grabec and Leskovar [5] on AE from machining of an aluminum alloy showed the signals to be produced by deformation and friction. Signals in the frequency range above 50 KHz were found to be rather weak. Even though this was explained to be due partly to low amplification, it is more likely due to the characteristics of the instrumentation used, especially that of the transducer and tool holder. Neither the depth of cut nor feed rate seemed to have any effect on the higher frequency components. It was on this basis that AE from metal cutting was deduced to be caused by friction between the tool and workpiece. Increasing speeds were found to increase the

high frequency components of the spectrum while decreasing the low frequency component. By observing specific spectral components, it was also observed that lower frequency components (about 2 KHz) showed an increase in amplitude with increasing flank wear while components around 43 KHz had decreasing amplitude. The main set back of this work is that the signal analysis was limited to the 0 to 100 KHz range where extraneous signals could have a strong influence, and most transducers have resonances.

Moriwaki [13] took the investigations a step further by studying the feasibility of detecting tool fracture using AE. Tool breakage was accelerated by rotating in a lathe, an alloy steel plate attached to the work holder. Both ceramic and P20 carbide cutting tools were used. Using both an accelerometer and a commercially available AE transducer, it was observed that the RMS value of the AE signal showed increased amplitudes when either chipping or fracture occurred while the acceleration signal showed very little change. On the other hand, large amplitude changes were observed in the acceleration signal during tool engagement and disengagement with the workpiece. The RMS AE signal was also found to increase gradually with machining time until failure occurred. This could be the result of increasing amounts of internal microcracks that ultimately culminated into final fracture. At certain instances when high levels of AE indicated possible failure, inspection of the tool did not reveal either cracking or chipping. Signals generated by the ceramic tools at failure generally seemed to be higher in amplitude than those resulting from failure of carbide tools. However, failure data for ceramic tools showed a lot more scatter, and was attributed to the difficulty in identifying the cracks on them.

By monitoring the AE from both conventional transverse and dynamic rupture testing of notched tool materials, it was shown that the RMS value of the signal increased with an increase in the fractured area. However, the AE signal was not affected by the loading speed.

Further understanding of the AE as generated from the cutting process, and its relationship to process parameters was obtained as a result of a theoretical study that was undertaken by Kannatey-Asibu and Dornfeld [7,8,9] in which a quantitative relationship was developed between the RMS value of the emission signal and parameters of the orthogonal cutting process. The relationship was based on processes in the shear zone and chip-tool interface, which were considered as distinct sources of AE, neglecting the tool-work interface. For verification of the theory, AE signals were generated using a sharp high speed steel cutting tool for short periods to eliminate the influence of the tool-work interface. 6061-T6 aluminum and plain carbon steel in tubular form were used as workpieces. A strong correlation was obtained between experimental and theoretical results. The square of the RMS value of the emission signal was shown to increase with the strain rate of the cutting process. This was expected from the relationship developed and was mainly the

effect of the cutting speed. Likewise, the signal RMS value increased with the rake angle, and for the same cutting conditions, the intensity of signals generated from 1018 steel was greater than that from 6061-T6 aluminum.

Variation of the emission signal with chip-tool contact was also studied by using a tool with reduced but varied contact length and the results confirmed the existence of bulk deformation close to the cutting edge and sliding friction farther away from the edge. The point at which a change in slope of the AE-contact length curve occurred was used as an estimate of the length of sticking zone and results obtained were reasonable, in comparison with available data.

Because of the dependence of the AE signal on the process parameters, as indicated by the theoretical analysis, and also on the characteristics of the instrumentation, it became necessary to develop signal analysis techniques that would yield features that were insensitive to many of the system variables. Kannatey-Asibu and Dornfeld [10] used the distribution moments of the RMS signal as a basis for analyzing the signal. Since this required a knowledge of the signal distribution function, the β function was assumed to represent the signal. The skew and kurtosis of the sampled data calculated on this basis was found to be sensitive to the stick-slip transition for chip contact at the tool-chip interface, and also showed a correlation with flank wear, with the skew decreasing while the kurtosis increased with progress in flank wear. A plot of the two parameters of the β function against each other also showed a definite trend with wear.

AE signals are generated from several sources during machining, and some of these are not directly related to wear. Kannatey-Asibu [11] listed the major sources as being:

a. plastic deformation in the shear zone (primary zone),
b. deformation and sliding friction at the chip-tool interface (secondary zone),
c. rubbing of the newly machined workpiece surface on the tool flank (tertiary zone),
d. chip breakage and entanglement of continuous chips with the cutting tool and/or workpiece,
e. chipping and fracture of the cutting tool, and
f. possibly the impact of cutting fluid applied in jet form under considerable pressure.

The first three sources listed are illustrated in Fig. 2 and the signals from them are of the continuous type emission signals which appear steady and are of lower amplitude, whereas signals from tool fracture, chip breakage, and chip entanglement are of the burst type that appear as individual and distinct signals with high amplitude. Of the six possible sources listed, only three were considered to be directly related to wear. He then discussed the need for classifying between the various sources and the appropriateness of using pattern recognition concepts for

distinguishing between signals from the principal sources and thus detecting signals related to tool wear and tool breakage.

Another approach to distinguishing tool wear related information from chip noise was investigated by Lan and Dornfeld [14], and involved setting a threshold level for the RMS signal. Burst signals resulting from chip breakage or chip rubbing are generally of a higher amplitude than the continuous signals from normal cutting. Thus, by selecting a threshold value above the continuous signal level, all signals whose RMS value exceeded the threshold were considered chip signals. While this method is good for a given set-up, (including work and tool materials, geometry, and instrumentation), the dependence of the threshold setting on the instrumentation and process parameters would make it cumbersome to use in a variety of applications.

Experiments involving AE detection of both flank and crater wear during conventional machining of a 4340 steel with a carbide tool showed an increasing RMS trend with flank wear. However, it was found that once crater wear became significant, the rate of increase of the RMS value with flank wear decreased, suggesting a reduction in the energy of the AE signal with increasing cratering. This is most probably due to the reduction in cutting forces that accompanies cratering. Such a trend makes the correlation of the RMS value with wear difficult when crater wear is appreciable. Spectral analysis of signals generated at various levels of flank wear showed spectral components in the 80-150 KHz range to increase substantially with increasing flank wear.

The large amplitude signals generated as a chip breaks have been used for monitoring the form of chip-breaking during machining by Dornfeld and Lan [15]. Each significant burst signal was attributed to the breaking of a chip and the event rate was thus used as an indication of chip-breaking frequency. Measured values of chip-breaking frequency showed good correlation with AE event rate. The spectral characteristics of the forces were also analyzed, but did not seem to show consistent results, mainly because of the low frequencies involved, which were subject to interference from extraneous sources. Abrupt changes in the number of AE events above a threshold were found to give an indication of chip congestion or entanglement. On the basis of the preceding work, a control system was proposed that would be used to maintain a desired chip-breaking condition.

In studying tool breakage detection using AE, Kakino [16] deduced that AE generated as a result of plastic deformation in the sheer zones for a plain carbon steel machined with a P20 carbide tool had spectral components mainly below 100 KHz, while tool breakage generated signals with components between 100 and 300 KHz. Chip-clinging was suggested to generate signals similar in spectral components to the shearing process. Similar results were obtained for other tool and workpiece material combinations. On the basis of these results, a tool breakage detection system

was developed with signals below 100 KHz being filtered off after amplification. The remaining signal was envelope-demodulated and compared with a reference voltage. Signals whose amplitude exceeded the threshold voltage were considered to indicate tool breakage.

Kakino also suggested that the amplitude of AE signals detected at the time of tool fracture was approximately proportional to the square root of the fractured surface area. Also, by detecting AE from different locations on machine tools, he further suggested that the appropriate locations for the transducer were the tool post for the lathe; the spindle quill for drilling; and the spindle head for milling.

Iwasaki and Yonetsu [17] monitored gradual tool wear, tool fracture, and tool cracking using AE signal analysis. The AE signal was band-pass filtered in the 100 KHz - 1 MHz range, full-wave rectified, further low-pass filtered at 2 Hz, and then sampled for analysis. Their preliminary tests with carbide tools on medium and high carbon steels showed the AE amplitude to increase almost linearly with the cutting speed while the feed and depth of cut seemed to have no effect. It was noted, however, that for a different type of work material, specifically 4-6 brass, increasing the feed and depth of cut increased the AE signal amplitude. Flank wear studies revealed an increase in AE amplitude with progress in wear, but the relationship depended on the cutting speed, with steeper slopes being obtained at higher speeds. The characteristics of the power spectrum was also found to change with flank wear.

For inducing tool breakage, a workpiece with a 3 mm slot was used. Two methods were used for analyzing the AE signals. One involved comparing the AE signal level at consecutive points and considering the tool failed when the ratio of the signal amplitude exceeded a predetermined value. This ratio was found to be independent of the cutting conditions and the value of 1.8 was considered effective in detecting a minimum area of tool fracture surface of about 0.1 mm . The second method, which was not actually tested, involved setting the filter range to 300 KHz - 1 MHz to remove signals related to gradual wear. A plot of the amplitude of AE signal in this range versus the area of fractured surface showed an increasing trend for both carbide and ceramic tools. A major set back of the first method is that sudden changes in signal could also result from chip breakage and chip signals while the second method requires further testing. The initiation of cracks in the tool were also considered detectable by monitoring the AE count rate and its standard deviation, and both increased when cracks were initiated.

The detection of thermal cracking during machining was also studied by Kakino and his coworkers [18] using a 15 mm thick 1048 plain carbon steel that was machined on a lathe with an M20 carbide tool. Characteristic burst signals that were observed after machining for some time were found to be followed by thermal cracks. These burst signals had a greater concentration

of spectral components in the 100 - 300 KHz range than signals from normal machining. In comparison with AE from chipping, the signals associated with thermal cracking had a longer time constant and a greater AE amplitude per unit area. Good correspondence (linear on a log-log plot) was also found between the total area of thermal cracks and the time integral of AE signals above 100 KHz. The time at which thermal cracks first appeared was also found to decrease as the cutting speed increased.

In their study on tool fracture detection, Lan and Dornfeld [19] listed growth of the plastic zone; microcracking in the process zone near the crack tip; and extension of the primary crack as the three processes most closely related to AE. However, AE associated with the plastic zone and microcracking in the tool fracture process were considered low level and thus difficult to detect. A relationship was developed between AE and a crack propagating in the insert with constant velocity as:

$$(RMS)^2 \alpha \frac{\pi \sigma^2 L}{2E}$$

where

RMS = root mean square of the AE signal
σ = applied stress
L = crack length
E = Young's modulus.

The RMS value was used for characterizing the AE signal mainly because the raw AE signal due to fracture was considered difficult to distinguish from chip noise. However, the RMS signal response is much slower. In the machining of SAE 1018 and 4340 steels with a carbide tool, fracture of the tool was found to be accompanied by a high rise in AE signal amplitude, followed by a drop in the signal amplitude due to a period of non-cutting action immediately following tool breakage. Experimental results showed the square of the AE RMS signal to increase, but non-linearly with the sectional area of fracture. On studying the spectral characteristics, it was found that the signal at the time of fracture was predominantly in the 80 - 150 KHz range.

The feed and tangential forces were also found to be sensitive to tool breakage; however, only the tangential force was consistent in showing a drop after breakage. The feed force showed either an increase or decrease following breakage, depending on the cutting conditions. A similar behavior was observed for the RMS signal after chipping.

A major difference between AE and force measurement of tool failure was the fact that the AE signal level changes occurred at the instant of tool failure while the force level changes were only observable after the tool had broken or chipped off.

Uehara and Kanda [20] studied some of the fundamental aspects of AE generation during metal cutting and deduced that signals detected at the workpiece side and the tool side would be different because of reflections at the chip-tool interface and on the shear plane. Thus signals detected by a sensor mounted on the cutting tool would be mainly from the chip-tool interface and the tool-workpiece interface while those detected on the workpiece-side would be principally from the primary shear zone and the tool-workpiece interface. This was experimentally verified by comparing AE signals simultaneously recorded on the tool and workpiece sides. One other possible reason for this difference is the difference in the propagating medium characteristics, which would tend to modify the original signal in a different manner on either side. Three basic differences were reported:

1. Burst signals observed on the tool side but not on the workpiece side.

2. Burst signals on the workpiece side but not on the tool side.

3. Burst signals on both sides.

These were attributed to various modes of built-up-edge break-up. However, it appears these differences are rather due to the modes of chip-breakage. It was also observed that discontinuous and saw-toothed chips exhibited periodic bursts on the tool side and continuous signals on the workpiece side. The periodicity was then shown to correspond with the variation in forces arising from the chip segmentation.

Their study of the AE power spectrum showed variation of the AE signal spectrum with the workpiece material for signals detected on the workpiece side. The spectrum, however, did not show much influence from wear. On the other hand, signals detected on the tool side seemed to show a much greater effect of wear on the power spectrum.

Finally, Uehara and Kanda suggested that the mean AE signal amplitude increases linearly with increasing speed, depth of cut, and width of flank wear while the spectral characteristics of the AE signal was scarcely affected by the cutting speed and tool materials, for signals detected on the tool side.

Work done to date in general indicates that AE presents a powerful tool for studying the mechanics of the metal cutting process, in-process tool wear sensing, and tool breakage detection. However, as stated by Dr. A. A. Pollock, formerly of Dunegan/Endevco, [21], "Signal interpretation is currently recognized as the most important frontier of AE technology. An empirical approach can often be applied successfully to a simple system or by a sufficiently experienced operator. But there is a constant demand for more rigorous and precise ways of interpreting AE.....". Such an analysis is essential if the

technique is to be applicable with greater reliability and accuracy to tool failure monitoring.

APPENDIX B

A Transport-Diffusion Equation in Metal Cutting and its Application to Analysis of the Rate of Flank Wear

E. Kannatey-Asibu, Jr.
Assist. Professor,
Department of Mechanical Engineering
and Applied Mechanics,
The University of Michigan,
Ann Arbor, Mich. 48109

A two-dimensional transport-diffusion equation is derived for diffusion in metal cutting by an extension of Fick's second law. The analysis considers the dynamics of the cutting process and thus offers a comprehensive representation of the diffusing species in the workpiece and the chip. A relationship for the rate of flank wear is derived considering adhesion and diffusion as the major modes of wear on the tool flank. It is based on the mechanics of the wear process, friction and diffusion, taking into account the regenerative effects of wear, temperature, and friction force. Based on the simulated results of the analysis, a new criterion is proposed for determining tool life.

Introduction

Analyses of cutting tool wear have traditionally emphasized flank wear more than crater wear, and the reason is the more direct influence flank wear has on the quality of the product. The onset of crater wear results in a change in the mechanics of the cutting process (the effective rake angle and the chip-tool contact length change) and also reduces the amount of force that the tool can withstand. Flank wear, on the other hand, has a three-fold influence. It results in:

(*a*) changes in the mechanics of the process,
(*b*) an increased tendency for chatter, and
(*c*) changes in the dimensions of the product.

Thus, as an initial step, the current analysis is restricted to wear on the flank of the cutting tool.

A number of analyses of wear in the cutting process have been undertaken over the years, and among those directly related to the current analysis are the works of Bhattacharyya and Ham [1], Rubenstein [2], Koren [3], Koren and Lenz [4], and Bhattacharyya and Ghosh [5]. Flank wear analyses are often limited to adhesive wear, diffusion being considered only in crater wear. A notable exception is the work of Koren [3], and Koren and Lenz [4]. Their analysis takes into account both abrasive (mechanically activated) and diffusion (thermally activated) wear, and considers the regenerative effects of wear and temperature or forces as a simple control system with positive feedback. In this paper adhesion is considered as the mechanically activated process.

This limits the applicability of the wear rate model to be developed since there are several other mechanisms that produce either wear or lead to tool failure, according to Trent [6]. In fact, Wright [7] specifically lists the seven major wear mechanisms as adhesion, abrasion, fracture, oxidation and subsequent adhesion, superficial plastic deformation, diffusion, and plastic collapse of the cutting edge. Furthermore, he emphasizes the fact that the mechanism that dominates in a given situation will depend on the work-tool combination, and several examples are given, supported by experimental work where individual or combinations of the listed mechanisms predominate for various conditions.

Consequently, no single model can adequately describe the wear behavior in all situations and it would seem appropriate to model the individual mechanisms or in combinations that are likely to occur together so that the appropriate model can be used for any given situation. An extensive analysis of the conditions that would result in tool failure by deformation has been done by Wright [12].

For conditions where adhesive wear is important, it predominates in the intermediate steady-state stages, but the regenerative effects of wear and temperature makes diffusion a considerable factor in the later stages and definitely predominant in the accelerated wear region. There is a critical temperature at which accelerated wear begins. Below that temperature, flank wear increases uniformly with time. Above that temperature, the wear increases exponentially with temperature. The exponential rise in wear above the critical temperature is due to the dominating influence of diffusion. The analysis in this paper incorporates the interdependence of the wear, forces, and temperature, and is based on the mechanics of the wear process, friction, and diffusion.

In optimization of the cutting process, the tool life that will optimize the process is not known beforehand, even though it provides the upper limit of the criterion integral. An aspect of tool wear that is essential for optimization is thus the rate at which the tool is wearing off. This analysis is thus not directed toward producing another form of the Taylor tool life

Contributed by the Production Engineering Division for publication in the JOURNAL OF ENGINEERING FOR INDUSTRY. Manuscript received at ASME Headquarters, March 30, 1984.

equation, but an expression for the rate of tool wear that can be suitably used in the optimization process.

Diffusion Flank Wear

Analysis of diffusion wear in metal cutting often involves direct invocation of Fick's Laws:

$$\text{Law I} \qquad J = -D\frac{\partial c}{\partial x} \tag{1a}$$

$$\text{Law II} \qquad \frac{\partial c}{\partial t} = \frac{\partial}{\partial x}\left(D\frac{\partial c}{\partial x}\right) \tag{1b}$$

These equations were essentially derived for systems where there is no relative sliding motion between the two surfaces across which diffusion is occurring and therefore, cannot correctly describe the diffusion process in the metal cutting process. Not only is the process two-dimensional for orthogonal cutting, it also involves bulk motion of material in a direction virtually perpendicular to the general direction of diffusion. In the following section, an equation is derived that takes into consideration both the diffusion and bulk motion processes, and incorporates the two-dimensional nature of the orthogonal system.

2.1 The Transport-Diffusion Equation in Metal Cutting. For an element 1234 of unit thickness (z-direction) on the flank side of the cutting tool in the orthogonal system shown in Fig. 1, the respective coordinates and concentrations at its four corners are:

1.	(x,y)	c
2.	$(x+\Delta x,y)$	$c+\frac{\partial c}{\partial x}\Delta x$
3.	$(x+\Delta x,y+\Delta y)$	$c+\frac{\partial c}{\partial x}\Delta x+\frac{\partial c}{\partial y}\Delta y$
4.	$x,y+\Delta y$	$c+\frac{\partial c}{\partial y}\Delta y$

As a result of the varying diffusion and transport rates into and out of the element, there is a buildup (or loss) of the diffusing species inside the element with time. There is no bulk motion of atoms across planes 1-2 and 4-3. Thus the flux of atoms across 1-2 is only by diffusion and is given as:

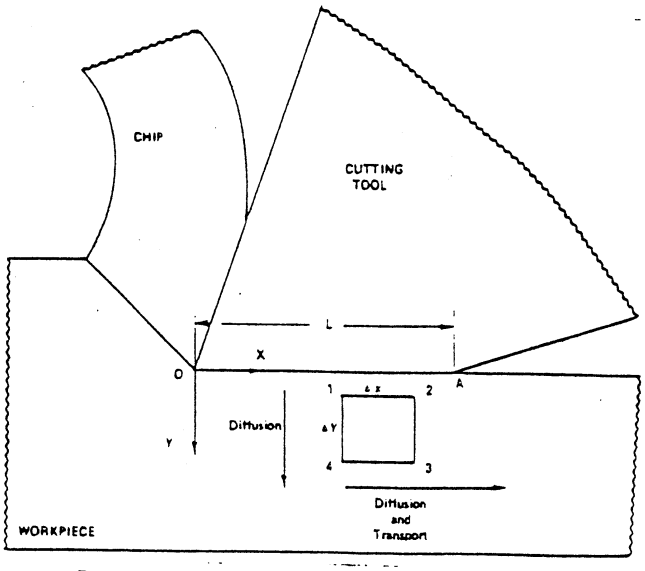

Fig. 1 Diffusion and transport element in metal cutting

$$J_{1y} = -D\frac{\partial c}{\partial y}\Delta x \text{ atoms per unit time} \tag{2}$$

and that across 4-3 is:

$$J_{2y} = J_{1y} + \frac{\partial J_{1y}}{\partial y}\Delta y$$

$$= -D\frac{\partial c}{\partial y}\Delta x - \frac{\partial}{\partial y}\left(D\frac{\partial c}{\partial y}\Delta x\right)\Delta y \tag{3}$$

Since there is transport across planes 1-4 and 2-3 due to the motion of the workpiece, flux across these planes include both diffusion and transport. For 1-4 we have:

$$J_{1xD} = -D\frac{\partial c}{\partial x}\Delta y \qquad \text{due to diffusion}$$

$$J_{1xT} = V\Delta y\left(c+1/2\frac{\partial c}{\partial y}\Delta y\right) \qquad \text{by transport}$$

Therefore,

$$J_{1x} = -D\frac{\partial c}{\partial x}\Delta y + V\Delta y\left(c+1/2\frac{\partial c}{\partial y}\Delta y\right) \tag{4}$$

and across 2-3:

Nomenclature

a = constant exponent
A = area of welded asperity joints
b = width of cut
c = concentration of diffusing species
C_o = concentration of diffusing species at the tool-work interface
D = diffusion coefficient
f = weight percentage of diffusing species in the tool material
F_t = thrust force
F = friction force on tool flank
G = specific weight of the workpiece material
h = height of welded joint torn off in shear
Δh = height of tool material removed in time Δt
H_w = penetration hardness of the workpiece
H_t = tool hardness
J = flux of diffusing atoms (atoms per unit time)
k_w = thermal conductivity of the workpiece
K, K_i = constants
L = wear land on the tool flank
m = atomic weight of the diffusing species
n = number of welded asperity joints
P_m = apparent contact pressure on tool flank
P_o = probability that a sizable wear particle of the harder material be formed
Q = activation energy for diffusion
R = gas constant
t = time
U = volume of asperity joint torn off
V = cutting speed
$dVol_t$ = change in volume of tool material due to flank wear
x = coordinate axis along the tool flank workpiece interface
y = coordinate axis into the workpiece
Θ = temperature
α = rake angle
α_w = thermal diffusivity of workpiece
γ = clearance angle
μ = coefficient of friction on tool flank
ρ_t = density of tool material
ρ_w = density of work material

$$J_{2xD} = J_{1xD} + \frac{\partial J_{1xD}}{\partial x}\Delta x$$

$$= -D\frac{\partial c}{\partial x}\Delta y - \frac{\partial}{\partial x}\left(D\frac{\partial c}{\partial x}\Delta y\right)\Delta x$$

$$J_{2xT} = J_{1xT} + \frac{\partial J_{1xT}}{\partial x}\Delta x$$

$$= V\Delta y\left(c + 1/2\frac{\partial c}{\partial y}\Delta y\right) + V\Delta y\left(\frac{\partial c}{\partial x} + 1/2\frac{\partial^2 c}{\partial x \partial y}\Delta y\right)\Delta x$$

Therefore,

$$J_{2x} = -D\frac{\partial c}{\partial x}\Delta y - \frac{\partial}{\partial x}\left(D\frac{\partial c}{\partial x}\Delta y\right)\Delta x$$

$$+ V\Delta y\left(c + 1/2\frac{\partial c}{\partial y}\Delta y\right) + V\Delta y\left(\frac{\partial c}{\partial x} + 1/2\frac{\partial^2 c}{\partial x \partial y}\Delta y\right)\Delta x \quad (5)$$

The net flux into the element is obtained from equations (2) to(5) as:

$$J = (J_{1x} - J_{2x}) + (J_{1y} - J_{2y})$$

$$= \frac{\partial}{\partial x}\left(D\frac{\partial c}{\partial x}\right)\Delta x\Delta y + \frac{\partial}{\partial y}\left(D\frac{\partial c}{\partial y}\right)\Delta x\Delta y - V\frac{\partial c}{\partial x}\Delta x\Delta y \quad (6)$$

with third order elements removed. The rate of change of concentration (atoms per unit volume per unit time) in the element is obtained by dividing both sides of the equation by the elemental volume $\Delta X \cdot \Delta Y \cdot 1$ and gives:

$$\frac{\partial c}{\partial t} = \frac{\partial}{\partial x}\left(D\frac{\partial c}{\partial x}\right) + \frac{\partial}{\partial y}\left(D\frac{\partial c}{\partial y}\right) - V\frac{\partial c}{\partial x} \quad (7)$$

and for a space invariant diffusion coefficient, equation (7) becomes:

$$\frac{\partial c}{\partial t} = D\frac{\partial^2 c}{\partial x^2} + D\frac{\partial^2 c}{\partial y^2} - V\frac{\partial c}{\partial x} \quad (8)$$

A complete analysis of the diffusion problem in orthogonal metal cutting should thus be based on equation (8). A solution of equation (8) will produce a complete representation of the state of the diffusing species in the workpiece and chip (with appropriate modification of the velocity term and axes rotation). Due to the complex boundary conditions that pertain in metal cutting, a closed form analytical solution will be rather difficult to obtain and numerical methods will inevitably have to be used for a complete solution. However, as a first step, simplifying assumptions will be made that will render a closed form solution feasible in the following analysis.

2.2 Diffusion Wear Model. Two basic assumptions are used in the development of the flank wear model due to diffusion.

1 A uniform temperature distribution exists along the tool flank-workpiece interface, i.e., in the x-direction, Fig. 1. The temperature, however, varies in the y-direction, i.e., into the workpiece away from the flank. This assumption might sound a little paradoxical at first. However, as shown in [8], the temperature variation along the interface is drastic only in the initial stages of the cut, but then tends to be more uniform with time or as wear progresses, when diffusion wear becomes significant.

2 The concentration of the diffusing species is constant at the tool-work interface and can be denoted as C_o. In the workpiece material close to the interface, the concentration is zero close to the edge of the cutting tool (since the atoms that previously diffused into the workpiece have been removed as that part of the workpiece forms the chip during the next rotation and is removed) and increases to a maximum (not necessarily C_o) at the end of the flank land.

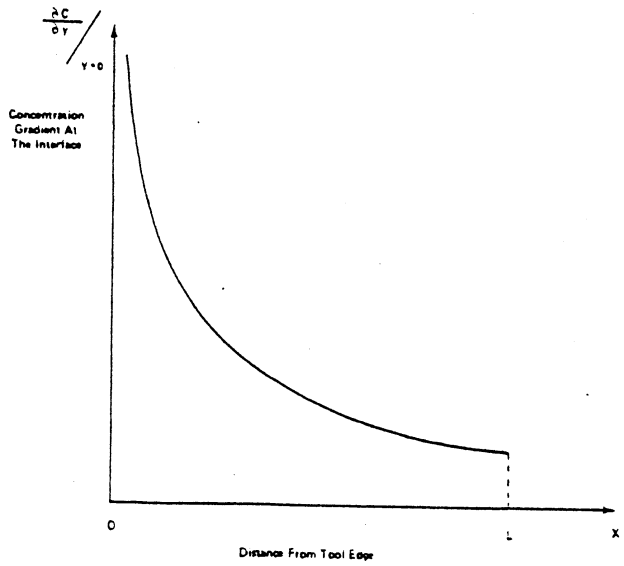

Fig. 2 Variation of the concentration gradient at the tool flank—workpiece interface

To get an idea of the validity of the latter assumption, let us consider the one-dimensional form of equation (8), and estimate the depth of diffusion (y-direction) in a planar element (perpendicular to the x-direction), by the time it moves from the tool edge to the end of flank land ($x = 0$ to $x = L$). To further simplify matters, the workpiece is considered stationary. This will tend to overestimate the depth, and that is preferable. Also, the diffusion coefficient, D, is taken as constant, based on its value at the interface where the temperature is maximum. Even though D will vary into the workpiece, the interface value will again overestimate the depth of diffusion. The general solution of equation (8) for the one-dimensional case with a stationary interface is obtained [9, 10] as:

$$c = C_o\left[1 - \mathrm{erf}\left(\frac{y}{2\sqrt{Dt}}\right)\right] \quad (9)$$

In the cutting process, the portion of the workpiece at the end of the flank land, point A, Fig. 1, has the maximum concentration of the diffusing species from the tool, Fig. 2. Thus, the time it takes a given element of the work to move from the tool edge to the end of the flank land will be used in estimating the depth, y, to which the tool material diffuses into the workpiece. A typical value for the wear land at failure is 0.3 mm [11]. Selecting a low cutting speed of 250 mm/s gives the time to move from the edge of the tool to the end of the flank land as:

$$t = \frac{0.3}{250} = 1.2 \times 10^{-3}\mathrm{s}$$

Using a value of the diffusion coefficient, D, of tungsten in steel at about 600°C from [5],

$$D = 10^{-10}\mathrm{mm}^2/\mathrm{s}$$

For the concentration, c, to be a significant percentage, say, 0.1 percent of that at the interface, the value of the error function in equation (9) has to be 0.999. That requires an error function argument of 2.327 [13], i.e.,

$$\frac{y}{2\sqrt{Dt}} = 2.327$$

$$y = 4.654\sqrt{Dt}$$

Substituting for the estimated values of D and t from above gives:

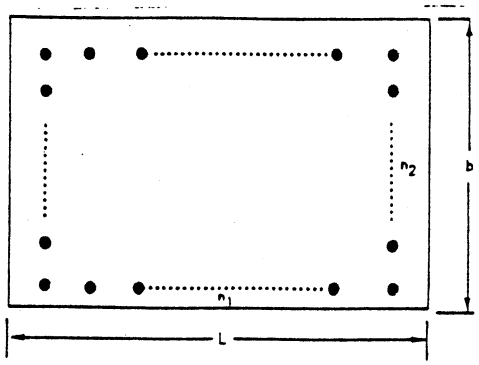

Fig. 3 Schematic of uniform asperity distribution at tool flank—workpiece interface

$$y = 4.654\sqrt{10^{-10}\times 1.2\times 10^{-3}}$$
$$= 1.61\times 10^{-6}\text{mm}$$
$$= 0.0016\ \mu\text{m}$$

The preceding calculation indicates that for tungsten to diffuse to any significant level in the next layer of material to be removed, the feed rate (or depth of cut in orthogonal cutting) has to be of the order of fractions of a micron. Thus, for all practical purposes, the assumption that the concentration of the diffusing species in the workpiece is zero at $x = 0$ is valid.

The coefficient of diffusion D is a function of temperature and is thus uniform along the interface, but may change with time, as temperature gradually varies with time due to increasing wear. Furthermore, the diffusion rate of the species from the tool into the workpiece is determined mainly by the concentration gradient at the interface. To obtain a closed form expression for the wear rate, the problem will be simplified by considering only diffusion into the workpiece (y-direction) and transport with the workpiece (x-direction). It is further assumed that the dynamic nature of the system is such that the concentration gradient $\partial c/\partial y/_{y=0}$ at any point along the interface does not change with time. It varies from infinity at $x = 0$ to a finite value at $x = L$. Thus, $\partial c/\partial y/_{y=0}$ is a function of x, Fig. 2, i.e.,

$$\left.\frac{\partial c}{\partial y}\right|_{y=0} = f(x) \tag{10a}$$

Even though the temperature, and thus the diffusion coefficient are assumed constant along the tool-work interface, the transport of material in the x-direction results in a variation of the concentration gradient along the interface (i.e., in the x-direction). The average concentration gradient over the interface is then given as:

$$\left.\frac{\partial c}{\partial y}\right|_{ave} = \frac{1}{L}\int_0^L \left(\frac{\partial c}{\partial y}\right) dx \tag{10}$$

From equation (9), we get:

$$\left.\frac{\partial c}{\partial y}\right|_{y=0} = -\frac{C_o}{\sqrt{\pi D t}} \tag{11}$$

The concentration gradient is dependent on time. However, the motion of the workpiece results in a change along the interface rather than at each position. Thus, t in equation (11) can be taken as the time it takes for an element of the workpiece to move from the edge of the tool to a position x. With a cutting speed V, then:

$$t = \frac{x}{V} \tag{12a}$$

And substituting in equation (11) gives:

$$\left.\frac{\partial c}{\partial y}\right|_{y=0} = -C_o\sqrt{\frac{V}{\pi D x}} \tag{12}$$

The average concentration gradient along the interface then becomes:

$$\frac{dc}{dy_{ave}} = -\frac{1}{L}\int_0^L C_o\sqrt{\frac{V}{\Pi D x}}\,dx$$
$$= -\frac{2C_o}{L}\sqrt{\frac{VL}{\Pi D}} = -2C_o\sqrt{\frac{V}{\Pi D L}} \tag{13}$$

Then by Fick's first law, the average flux rate is:

$$J_{ave} = -D\frac{dc}{dy_{ave}} = 2C_o\sqrt{\frac{VD}{\Pi L}}\ \text{atoms/mm}^2\text{-s}$$

The amount of tool material diffused across the interface per interval of time Δt is then given as:

$$d\text{Vol}_1 = b\cdot L\cdot\frac{m}{f\rho}J_{x=0}\Delta t = 2b\frac{m}{f\rho}C_o\sqrt{\frac{DVL}{\Pi}}\Delta t$$

$$= 2b\frac{m}{f\rho}C_o\sqrt{\frac{D_o V}{\Pi}}e^{-\left(\frac{Q}{2R(\Theta+273)}\right)}L^{1/2}\Delta t \tag{14}$$

Adhesive Wear Model

On the initiation of a cut, the finite roundness of the tool edge enables contact to be established between the tool flank and the workpiece. The contact pressure (apparent), P_m, is determined by the initial cutting conditions. As explained in the literature [14], contact is established by the welding together of asperities at the interface.

Let us consider the case where there are n_o welded asperities, each of cross-sectional area A_o at the beginning of the cut and which are uniformly distributed throughout the interface between the tool flank and the workpiece, Fig. 3. The asperity junctions are established by the asperities of the harder material pushing into the opposing asperities of the softer material until the surrounding material restrains further penetration. The two asperities then weld together under the high temperatures. If the initial thrust force acting on the tool flank is F_{io}, then the actual contact pressure, considering the actual area supporting the load, is a measure of the hardness of the softer material and is given by:

$$H_w = \frac{F_{io}}{n_o A_o} \tag{15}$$

where

H_w = penetration hardness of the softer material

Therefore,

$$n_O A_O = \frac{F_{io}}{H_w} \tag{16a}$$

In the general case as wear progresses, equation (16a) becomes:

$$nA = \frac{F_i}{H_w} \tag{16}$$

If the uniform asperity junction distribution at the tool-work interface shown in Fig. 3 has n_1 asperities along the length of the flank, then the number of asperities per unit length per row, $n_1{}^*$ is:

$$n_1{}^* = \frac{n}{n_2 L} = \frac{n_1}{L}$$

The number of asperities per row over a distance Δx is thus:

$$n_1{}^{**} = \frac{n_1}{L}\Delta x$$

As the tool and workpiece slide with respect to each other, old junctions are torn off and new ones are formed. For a tool moving with a velocity, V, the relative sliding distance, Δx, between the tool flank and workpiece sufrace in time Δt is:

$$\Delta x = V\Delta t$$

And the number of asperities per row over the length Δx becomes:

$$n_1^{**} = \frac{n_1}{L} V\Delta t \tag{17}$$

In time Δt, the number of times an asperity junction is broken and reformed, assuming n asperity junctions are formed at any one time, is therefore given by equation (17). If each joint that breaks results in the removal of a volume, U, of tool material, then the total volume, $d\text{Vol}_2$, removed in the interval Δt is:

$$d\text{Vol}_2 = U \cdot n \frac{n_1}{L} V\Delta t \tag{18}$$

From Fig. 3,

$$\frac{n_1}{n_2} = \frac{L}{b}$$

and since

$$n_1 \cdot n_2 = n,$$

$$\frac{L}{b} = \frac{n_1^2}{n} \quad \text{or} \quad n_1 = \left(\frac{nL}{b}\right)^{1/2}$$

Thus, equation (18) becomes:

$$d\text{Vol}_2 = U \cdot n \cdot \left(\frac{n}{Lb}\right)^{1/2} \cdot V\Delta t \tag{19}$$

The volume, U, is given by:

$$U = hA \tag{20a}$$

where

h is the characteristic height of the portion of the asperity removed.

According to Rabinowicz [15, 16], the volume of material removed is inversely proportional to its hardness. Since the joint cross-sectional area, A, is considered constant, the relationship is reflected in the height removed, i.e.,

$$h = \frac{K_o}{H_t}$$

or

$$h \cdot H_t = K_o \tag{20b}$$

In reality, since the asperity joints are not perfectly cylindrical in shape, the height, h, is a characteristic height, but its dependence on the asperity shape is neglected in the present analysis.

Substituting equation (20b) into (20a) gives:

$$U = K_o A \cdot \frac{1}{H_t} \tag{20}$$

From (19) and (20), we get:

$$d\text{Vol}_2 = K_o \cdot A \cdot n \cdot \left(\frac{n}{Lb}\right)^{1/2} \cdot V\Delta t \cdot \frac{1}{H_t}$$

and from (16),

$$d\text{Vol}_2 = K_o \cdot \frac{F_t}{H_w} \cdot \left(\frac{n}{Lb}\right)^{1/2} \cdot V\Delta t \cdot \frac{1}{H_t} \tag{21a}$$

Equation (21a) assumes that all the asperities form joints that result in shearing of asperities of the hard material. It is obvious that this will generally not be the case, and that joint sheairng is more likely to occur either at the interface or within the asperities of the softer material. However, there are occasions when weak areas of the harder material will result in shearing occurring through some asperities of the harder material. Let us indicate the probability that a sizable wear particle of the harder material be formed by P_o. Then equation (21a) becomes:

$$d\text{Vol}_2 = P_o K_o \frac{F_t}{H_w} \left(\frac{n}{Lb}\right)^{1/2} V\Delta t \frac{1}{H_t} \tag{21}$$

Estimates of P_o (also known as the wear coefficient) have been obtained by Rabinowicz [15-18].

Equation (21) gives the volume of tool material lost by adhesion in the interval Δt. The ratio (n/Lb), i.e., the number of asperity joints per unit area, is constant since the asperities are uniformly dispersed at the tool-work interface. The hardness of the tool material, however, depends on the cutting temperature and the dependence is regenerative, i.e., the increase in temperature is the result of progress in wear, which is further influenced by the temperature.

As explained earlier, the causality between the length of wear and the thrust force F_t is irreversible, i.e., the increase in F_t is due to an increase in the wear land and this is confirmed by earlier studies which show the flank forces increasing linearly with an increase in wear land [19, 20]. This also validates the assumption of near uniform distribution of the asperities. However, the hardness and temperature do vary as wear progresses. First, let us look at the influence of wear land on temperatures generated.

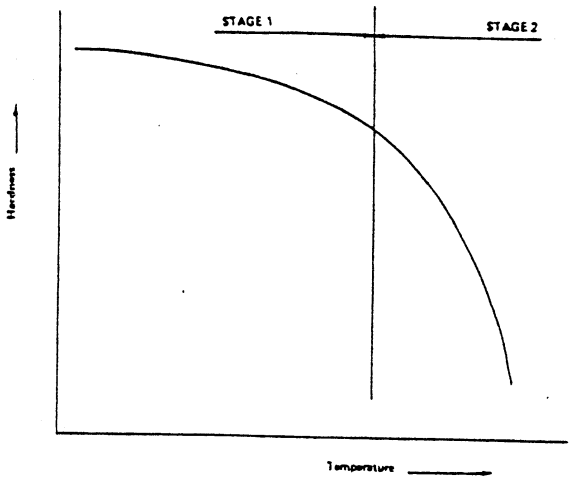

Fig. 4 Variation of tool material hardness with temperature

3.1 Wear Land and Flank Temperatures. The temperature rise at the interface between a square slider of side $2l$ and a rotating disk is given [22] as:

$$\theta = \theta_o + \frac{\mu F_t V\sqrt{\alpha_1}}{3.76l[1.125k_2\sqrt{\alpha_1} + k_1\sqrt{lV}} \tag{22a}$$

where

α_1 = thermal diffusivity

Subscript 1 refers to the disk, and subscript 2 refers to the slider.

At the high speeds used in machining,

$$k_1\sqrt{lV} >> 1.125k_2\sqrt{\alpha_1}$$

Thus equation (22a) reduces to:

$$\theta = \theta_o + \frac{\mu F_t\sqrt{\alpha_1} \cdot \sqrt{V}}{3.76lk_1\sqrt{l}} \tag{22b}$$

In adapting equation (22b) to the cutting process, we consider the apparent contact area between the contacting bodies and equate these for the two cases, giving:

$$(2l)^2 = bL$$

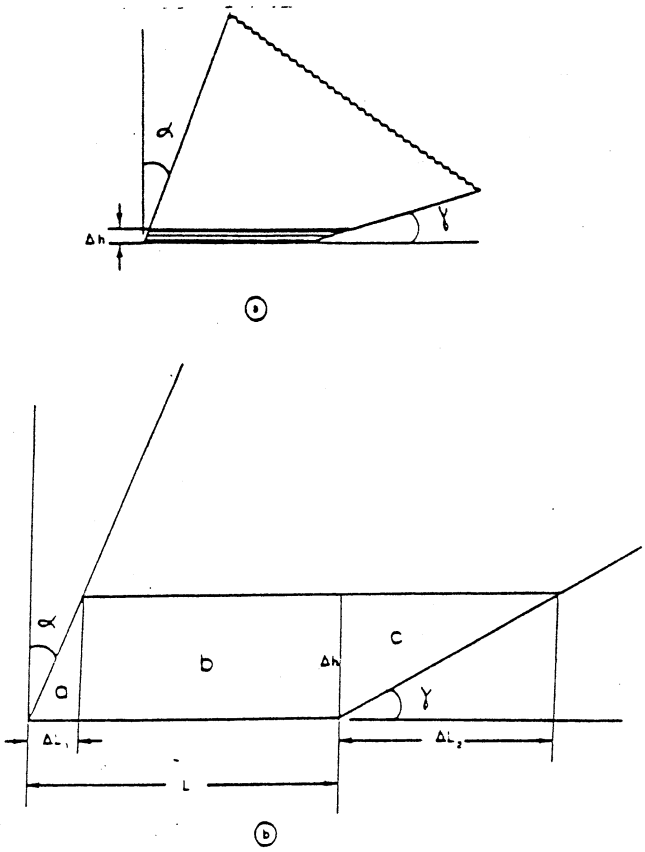

Fig. 5 Geometrical volume of tool material removed

or

$$l = 1/2\sqrt{bL}$$

Furthermore, due to the more massive nature of the heat sink in metal cutting, the temperature rise will be lower than predicted by equation (22*b*) by a factor of approximately 3. The final form of the temperature-wear land relationship is thus expressed as:

$$\theta = \theta_o + KL^{0.25} \tag{22}$$

where

$$K = \frac{0.251\alpha_w^{1/2}\mu P_m\sqrt{V}b^{0.25}}{k_w}$$

and α_w = workpiece thermal diffusivity.

The pressure P_m is based on the apparent contact area at the interface, and since the flank forces increase linearly with an increase in wear land [19, 20], despite changing temperatures, it can be considered constant. This is more clearly seen from the equation for P_m given as:

$$P_m = \frac{F_l}{bL}$$

where F_l increases linearly with L.

3.2 **Tool Hardness and Temperature.** The effect of the varying tool hardness with temperature is to vary the actual contact area, A, between the tool and the workpiece, and not the apparent contact area, bL. Consequently, the pressure P_m remains constant. The variation of the tool material hardness with temperature is generally of the form shown in Fig. 4, [21], and can be partitioned into two stages:

Stage 1—where the reduction in hardness with increasing temperature is not very great and where the wear process is mainly adhesive; and

Stage 2—where there is a drastic reduction in hardness for a small increase in temperature. This is the region where diffusion becomes the predominant mechanism. The onset of this stage signifies the beginning of the end of tool life.

The relationship between the hardness and temperature in Stage 1 can be expressed [2] as:

$$H = H_o\left(\frac{\theta}{\theta_o}\right)^{-o} = H_o\left(\frac{\theta_o}{\theta}\right)^{o} \tag{23}$$

Flank Wear Rate

From equations (14) and (21), the total volume of tool material removed in time Δt is given by:

$$d\text{Vol} = d\text{Vol}_1 + d\text{Vol}_2 = \left[P_oK_o\cdot\frac{F_l}{H_w}\left(\frac{n}{Lb}\right)^{1/2}\cdot V\cdot\frac{1}{H_l} + 2b\cdot\frac{m}{f\rho}\cdot C_o\sqrt{\frac{D_oV}{\Pi}}\cdot e^{-\left(\frac{Q}{2R(\theta+273)}\right)}L^{1/2}\right]\Delta t \tag{24a}$$

Substituting for H_l from equation (23) gives:

$$d\text{Vol} = \left[P_oK_o\cdot\frac{F_l}{H_w}\cdot\left(\frac{n}{Lb}\right)^{1/2}\cdot V\cdot\frac{\theta^o}{H_{lo}\theta_o^{\,o}} + 2b\cdot\frac{m}{f\rho}\cdot C_o\sqrt{\frac{D_oV}{\Pi}}\cdot e^{-\left(\frac{Q}{2R(\theta+273)}\right)}L^{1/2}\right]\Delta t \tag{24b}$$

and further substituting for θ from equation (22) gives:

$$d\text{Vol} = \left[P_oK_o\cdot\frac{F_l}{H_w}\cdot\left(\frac{n}{Lb}\right)^{1/2}\cdot V\cdot\frac{(\theta_o+KL^{0.25})^o}{H_{lo}\theta_o^{\,o}} + 2b\cdot\frac{m}{f\rho}\cdot C_o\sqrt{\frac{D_oV}{\Pi}}\cdot e^{-\left(\frac{Q}{2R(\theta_o-273+KL^{0.25})}\right)}L^{1/2}\right]\Delta t \tag{24}$$

The geometrical volume of tool material removed in time Δt is given by Bhattacharyya et al., [1] and briefly explained here. The shaded portion of Fig. 5(*a*) is the amount of tool material worn away during orthogonal cutting in the interval Δt, resulting in a reduction in the depth of cut Δh. Figure 5(*b*) is an enlargement of the shaded area. The volume of material removed, $d\text{Vol}$, is then given by:

$$d\text{Vol} = d\text{Vol}_a + d\text{Vol}_b + d\text{Vol}_c$$
$$= 1/2b(\Delta h)^2(\tan\alpha + \cot\gamma) + bL\Delta h - (\Delta h)^2\tan\alpha$$

and eliminating higher order terms,

$$d\text{Vol} = bL\Delta h = \frac{bL}{\cot\gamma - \tan\alpha}\cdot\Delta L = K_1L\Delta L \tag{25}$$

where

$$\Delta L = \Delta L_2 - \Delta L_1 = \Delta h(\cot\gamma - \tan\alpha)$$

and

$$K_1 = \frac{b}{\cot\gamma - \tan\alpha}$$

From equations (24) and (25), we get an expression for the rate of tool wear:

$$K_1L\Delta L = \left[P_oK_o\frac{F_l}{H_w}\left(\frac{n}{Lb}\right)^{1/2}V\frac{(\theta_o+KL^{0.25})^o}{H_{lo}\theta_o^{\,o}} + 2b\frac{m}{f\rho}C_o\sqrt{\frac{D_oV}{\Pi}}e^{-\left(\frac{Q}{2R(\theta_o+273+KL^{0.25})}\right)}L^{1/2}\right]\Delta t$$

which in the limit gives the wear rate:

Table 1 Typical material properties and cutting conditions

Variable	Value	Reference
V	3048 mm/s (600 fpm)	selected
γ	10 deg	selected
α	5 deg	selected
b	5.08 mm (0.2 in.)	selected
P_m	288 N/mm^2	[20], p. 77
$^*\mu P_m$	500 N/mm^2	[20], p. 77
H_w	1700 N/mm^2	[25], p. 223
ρ_w	7.8×10^{-6} kg/mm^3	[25], p. 145
ρ_t	15×10^{-6} kg/mm^3	[26], p. 457
k_w	45 w/m k	[25], p. 148
f	0.8	[5]
C_o	0.02	[5]
D_o	5000 mm^2/s	[24], p. 66
Q	79.5 kcal/mole	[24], p. 66
R	1.987 cal/mole K	
P_o	10^{-6}	[15]
$^*\frac{n}{Lb}$	10^4/mm^2	[16, 22]
$^*h$	10^{-3}	[16, 22]
$^*K_o$	$H_w h$	[21]
a	0.055	

$$\frac{dL}{dt} = K_1^{\prime}\frac{F_t}{Lb}V\frac{(\theta_o+KL^{0.25})^a}{H_{to}\theta_o{}^a} + K_3\sqrt{V}e^{-\left(\frac{Q}{2R(\theta_o+KL^{0.25})}\right)}L^{-1/2}$$

$$\theta_o = \theta_o + 273$$

Now considering that the apparent contact pressure is given by

$$P_m = \frac{F_t}{bL}$$

we have

$$\frac{dL}{dt} = K_2 V(\theta_o+KL^{0.25})^a + K_3\sqrt{V}e^{-\left(\frac{^*Q}{2R(\theta_o+KL^{0.25})}\right)}L^{-1/2} \quad (26)$$

where the constant

$$K_2 = P_o\frac{(\cot\gamma-\tan\alpha)K_oP_m}{H_wH_{to}\theta_o{}^a}\left(\frac{n}{Lb}\right)^{1/2}$$

$$K_3 = 2\frac{m}{f\rho}(\cot\gamma-\tan\alpha)C_o\sqrt{\frac{D_o}{\pi}}$$

$$K = \frac{0.251\alpha_w{}^{1/2}\mu P_m\sqrt{V}b^{0.25}}{k_w}$$

Example

The purpose of the following example is to get an idea of the range of wear rates predicted by the preceding analysis and the trends they portray. A typical workpiece material will be considered—AISI 1045 steel with a steel cutting grade tungsten-carbide cutting tool (WC-TiC-TaC-Co). Since the material property values are taken from various sources, these are listed in Table 1 along with the source references. Cutting is assumed to be orthogonal to conform with the analysis. Selection of values for the variables denoted with an asterisk is explained below.

• n/Lb—The number of asperities per unit area can be accurately obtained for a given system using an electron microscope. However to obtain an estimate for the present calculations, we consider the results of Bowden and Tabor [22] which indicate that under loads similar to those incurred in metal cutting, the average size of an asperity is of the order of 0.01 mm. Assuming the asperities are spaced at a distance equal to their diameter, then the number of asperities per square millimeter is 10^4, i.e.

$$\frac{n}{Lb} = 10^4 \text{ asperities/mm}^2$$

• h—The height of the asperities were also found to be of the order of 5×10^{-3} mm for the unloaded surface [22]. Assuming the height torn off is 20 percent of the unloaded height, then

$$h \approx 10^{-3}\text{mm}$$

• $\mu P_m = \frac{F_c}{F_T}\cdot\frac{F_T}{Lb} = \frac{F_c}{Lb} = 51 \text{ kg/mm}^2 = 500\text{N/mm}^2$

• K_o—From equation (20b), $K_o = H_t\cdot h$

Thus K_o is replaced with $H_{to}\cdot h$

Using the sample values from Table 1, the wear rate equation is obtained as:

$$\frac{dL}{dt} = 0.0792\times10^{-6}\times V(25+13\sqrt{V}L^{0.25})^{0.055} +$$

$$0.137\times10^6\times\sqrt{V}\times e^{-\left(\frac{20000}{298+13\sqrt{V}L^{0.25}}\right)}\times L^{-1/2}$$

The first term on the right is the contribution to the wear rate due to adhesion and the second term is the contribution due to diffusion. Both terms are plotted along with the total wear rate against the wear land for various speeds and wear land rates in Fig. 6.

Discussion

Some of the data used in the example are approximate, and thus the wear rates obtained must not be taken as absolute values. The significant aspects of the results are the trends they indicate. At very low wear values, i.e. in the initial stages of a cut, the rate of diffusion wear is insignificant compared to the adhesive wear rate. However, the diffusion rate of wear increases rapidly until it becomes the dominating mechanism after a certain amount of wear. On the other hand, the adhesive wear rate remains relatively constant. In reality, the adhesive wear rate should reduce after the tool hardness enters the rapid deterioration stage, but since that occurs after the wear process is predominately diffusive, it is not incorporated in the wear rate equation.

The value of wear land at which diffusion begins to dominate depends on the cutting speed, being approximately 0.28 mm at a speed of 3.048 m/s (600 fpm), and increasing as the cutting speed decreases. Comparing the crossover point of 0.28 mm with the recommended criterion for tool life of 0.3 mm [11], it might be expected that the time at which the rate of wear due to diffusion exceeds that due to adhesion could be used as a criterion for tool life as suggested in [23]. In such a case, then, it would only be necessary to estimate the parameters of the wear rate equation to determine when a tool should be changed. Such a criterion would be appropriate for situations where a tool needs to be used until it almost fails, and also where adhesion and diffusion are the dominant mechanisms for wear.

The advantage of using such a wear rate criterion can be better understood by considering the wear land at which the crossover occurs and also the wear rate at that instant for various speeds, Figs. 7 and 8. At a speed of 2.032 m/s (400 fpm), the wear land and wear rate at crossover are 0.67 mm and 0.46×10^{-3} mm/s, respectively, whereas those at 4.064 m/s (800 fpm) are 0.16 mm and 1.0×10^{-3} mm/s, respectively. As mentioned earlier, crossover occurs at shorter and shorter wear lands as the cutting speed increases, while the wear rate at that time increases. What this means is that, in the conventional method of using a fixed wear land to determine tool life, a substantial amount of the life of the tool could be left at the time it is removed from service, especially at low speeds. However, by using the wear rate criterion, the tool could be used for a substantially longer period of time at lower speeds than the time predicted by the fixed wear land

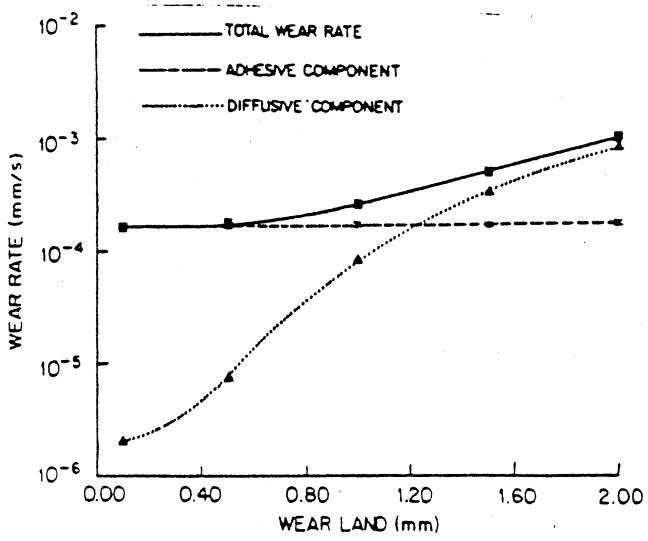

Fig. 6(a) Cutting speed: 1.524 m/s (300 fpm)

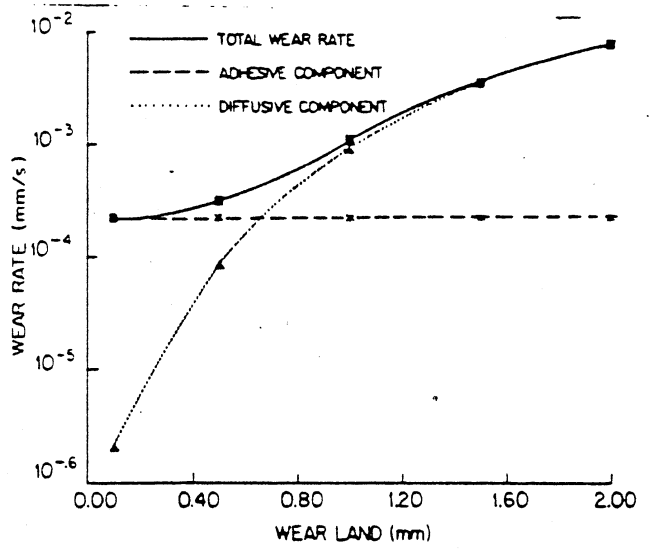

Fig. 6(b) Cutting speed: 2.032 m/s (400 fpm)

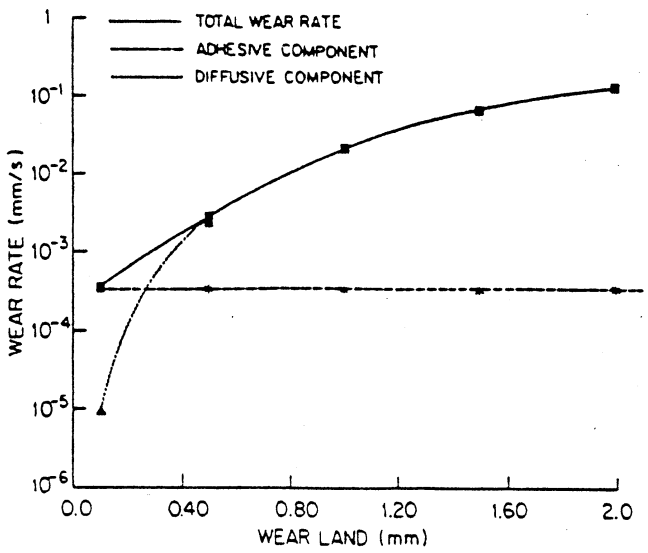

Fig. 6(c) Cutting speed: 3.048 m/s (600 fpm)

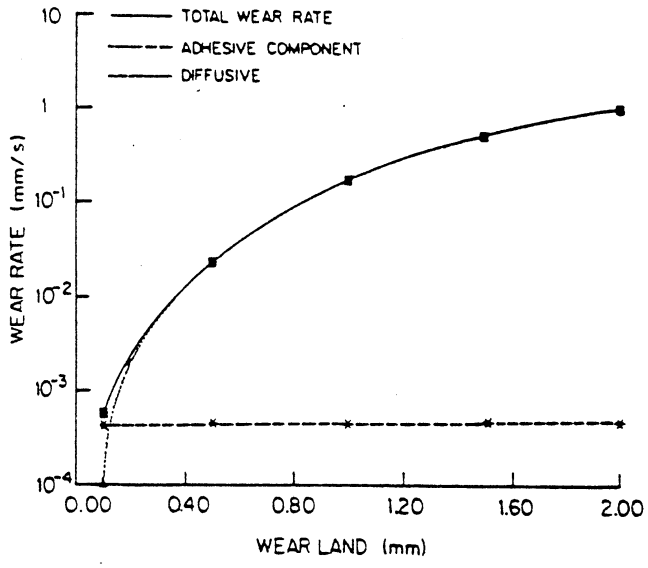

Fig. 6(d) Cutting speed: 4.064 m/s (800 fpm)

Fig. 6 Wear rates at various levels of wear land

criterion. Even more substantial savings could be realized by using a fixed wear rate value rather than the crossover point since the wear rate at a fixed wear land increases almost exponentially with speed, Fig. 9. This type of criterion would be most useful in situations where tolerances are not critical to the process and also the machine tools are rigid enough to curtail chatter arising from excessive wear. Even with finishing cuts on short workpieces, the wear rate criterion could be used provided part dimensions are measured after machining and the depth of cut is adjusted to account for dimensional changes resulting from tool wear, and also provided surface finish does not deteriorate too rapidly.

Concluding Remarks

Fick's second law of diffusion is extended to account for the dynamics of the diffusing species in metal cutting. The end result is a two-dimensional transport-diffusion equation which is more representative of the state of the diffusing species either in the chip or the workpiece.

Furthermore, a relationship is derived for the rate of flank wear on the basis that tool wear occurs primarily by adhesion (during steady-state wear) and diffusion. The objective has not been to obtain another form or improved version of Taylor's Law, but to enable a prediction of the onset of the tertiary stage of wear, with the reasoning that this stage is entered when diffusion begins to dominate the wear process.

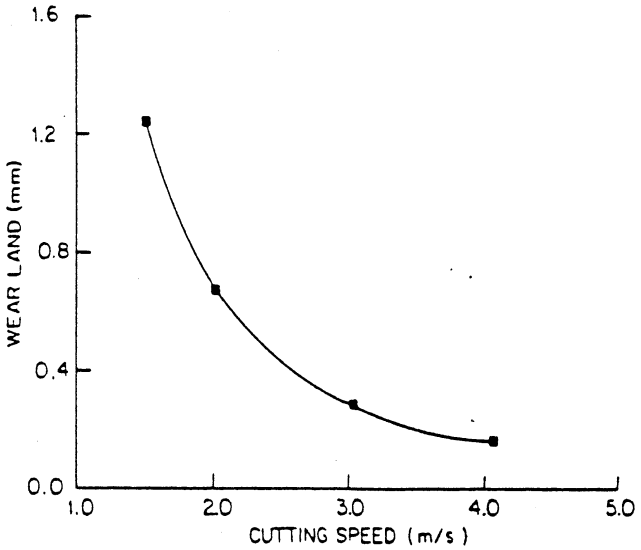

Fig. 7 Variation of the wear land at the crossover point with cutting speed

In this respect, the cutting speed is considered invariant (based on the predetermined speed for a particular operation). Even though in optimal control of the cutting process the input speed will change during the operation, constraints imposed in optimization will often penalize excessive deviations in the input.

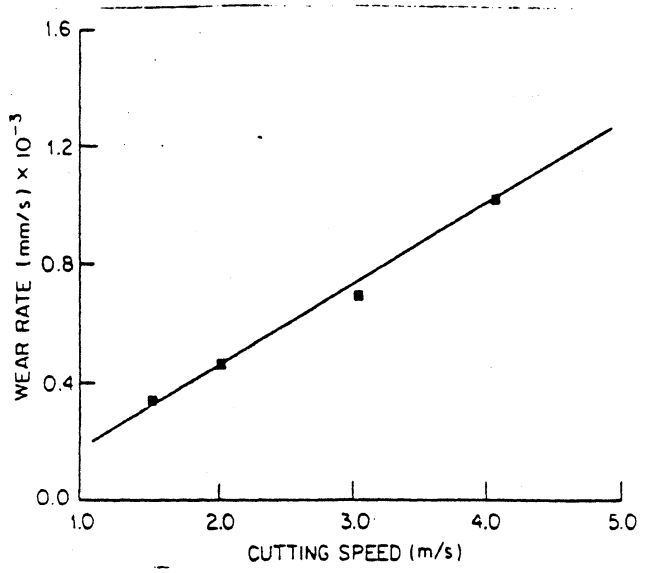

Fig. 8 Variation of the wear rate at the crossover point with cutting speed

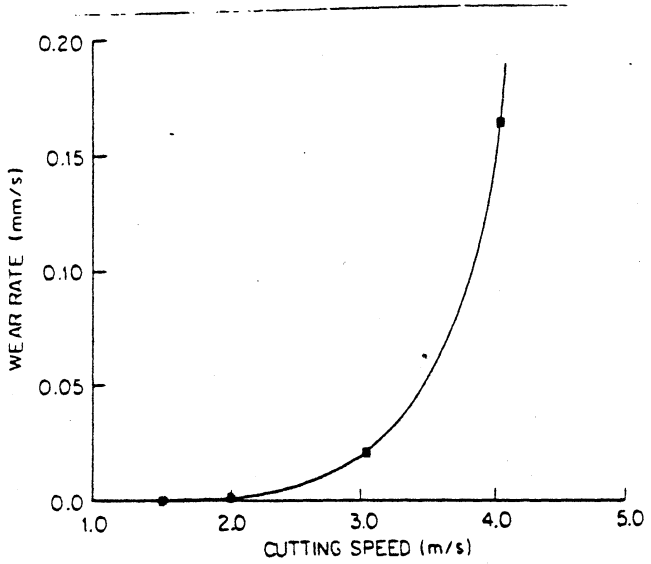

Fig. 9 Variation of the wear rate at a wear land of 1.0 mm with cutting speed

The analysis, as it presently stands, neglects the wear contribution due to abrasion and also the transfer of heat from the shear zone and chip-tool interface to the tool flank.

An example calculation of the wear rates based on typical cutting conditions shows that the model conforms reasonably well with general trends in practice where there is a period of uniform wear rate, followed by a period of rapid tool deterioration which, as the model suggests, begins to occur soon after diffusion wear becomes predominant. Using this model, therefore, a criterion could be developed for tool life based on the relative magnitudes of the rates of adhesive wear and diffusion wear.

Such a criterion will permit, as shown by the example, a more efficient use of the tool since the tool would be used over a longer period of time at lower speeds than would ordinarily be done using the fixed wear land criterion. Moreover, as a result of its simplicity and generality, the model is highly suited for use in the metal cutting process control.

Another important aspect of the wear rate criterion would be its use in the development of a tool wear sensor. Current and past efforts have been mainly aimed at developing a sensor that will measure the absolute value of wear. After extensive research in this area, the author is convinced that a more appropriate approach will be to develop a sensor that tracks the rate of change of wear rather than wear itself, since the absolute values of signals used (for indirect measurement) are more sensitive to variations in process parameters.

Acknowledgment

I am very grateful to the reviewers of this paper, and also to Professor Ehud Lenz (Technion, Israel, and currently on sabbatical at The University of Michigan) for their constructive comments and suggestions which have proven very useful to the long-term goals of this project. My appreciation also goes to Erdal Emel, a graduate student, for some of the drawings and to Mrs. Sheryll Marshall for the excellent work in typing the manuscript. Finally, my gratitude to the Department of Mechanical Engineering and Applied Mechanics of The University of Michigan for continued support of the project.

References

1 Bhattacharyya, A., and Ham, I., "Analysis of Tool Wear, Part 1: Theoretical Models of Flank Wear," ASME JOURNAL OF ENGINEERING FOR INDUSTRY, Vol. 91, 1969, pp. 790-798.

2 Rubenstein, C., "An Analysis of Tool Life Based on Flank-Face Wear, Part 1: Theory," ASME JOURNAL OF ENGINEERING FOR INDUSTRY, Vol. 98, 1976, pp. 221-226.

3 Koren, Y., "Flank Wear Model of Cutting Tools Using Control Theory," ASME JOURNAL OF ENGINEERING FOR INDUSTRY, Vol. 100, 1978, pp. 103-109.

4 Koren, Y., and Lenz, E., "Mathematical Model for the Flank Wear while Turning Steel with Carbide Tools," *Proc. CIRP Seminars on Manufacturing Systems*, Vol. 1, No. 2, 1972, pp. 127-137.

5 Bhattacharyya, A., and Ghosh, A., "Diffusion Wear of Cutting Tools," *Proc. 5th Int'l MTDR Conf.*, 1964, pp. 225-242.

6 Trent, E. M., "Tool Wear and Machinability," *Inst. of Production Engineers Journal*, Vol. 28, No. 3, 1959, pp. 105-130.

7 Wright, P. K., "Correlation of Tool Wear Mechanisms with Slip-Line Fields for Cutting," *Wear of Materials-1981*, Ludema, K., (Ed.), ASME, New York, 1981, pp. 482-488.

8 Levy, E. K., Tsai, C. L., and Groover, M. P., "Analytical Investigation of the Effect of Tool Wear on the Temperature Variations in a Metal Cutting Tool," ASME JOURNAL OF ENGINEERING FOR INDUSTRY, Vol. 98, 1976, pp. 251-257.

9 Guy, A. G., "Transport in Materials," *Introduction to Materials Science*, McGraw-Hill, New York, 1971, pp. 247-295.

10 Barret, C. R., Nix, W. D., and Tetelman, A. S., "Kinetics," *The Principles of Engineering Materials*, Prentice-Hall, Englewood Cliffs, N.J., 1973, pp. 144-192.

11 Boothroyd, G., "Tool Life and Tool Wear," *Fundamentals of Metal Machining and Machine Tools*, McGraw-Hill, New York, 1975, pp. 108-124.

12 Yen, D. W., and Wright, P. K., "Adaptive Control in Machining—A New Approach Based on the Physical Constraints of Tool Wear Mechanisms," ASME JOURNAL OF ENGINEERING FOR INDUSTRY, Vol. 105, 1983, pp. 31-38.

13 Tables of Probability Functions, Vol. 1, 1941, National Bureau of Standards.

14 Finnie, I., and Shaw, M. C., "The Friction Process in Metal Cutting," *Transaction ASME*, Vol. 78, 1956, pp. 1649-1657.

15 Rabinowicz, E., "Adhesive Wear Values as Affected by Strength Fluctuations," *Wear of Materials-1981*, ASME, New York, 1981, pp. 197-201.

16 Rabinowicz, E., "Adhesive Wear," *Friction and Wear of Materials*, Wiley, New York, 1965, pp. 125-166.

17 Rabinowicz, E., "An Adhesive Wear Model Based on Variations in Strength Values," *Wear*, Vol. 63, 1980, pp. 175-181.

18 Rabinowicz, E., "The Wear Coefficient-Magnitude, Scatter Uses," ASME *Journal of Lubrication Technology*, Vol. 103, 1981, pp. 188-194.

19 Kobayashi, S., and Thomsen, E. G., "The Role of Friction in Metal Cutting," ASME JOURNAL OF ENGINEERING FOR INDUSTRY, Vol. 83, 1961, pp. 324-332.

20 Koren, Y., "Dynamic and Static Optimization of the Cutting Process," *1st NAMR Conference*, Hamilton, May 1973, pp. 67-94.

21 Swinehart, H. J., (Ed.), "Tool Properties," *Cutting Tool Material Selection*, ASTME, 1968.

22 Bowden, F. P., and Tabor, D., "Area of Contact Between Solids," *The Friction and Lubrication of Solids*, Oxford University Press, London, 1954, pp. 5-32.

23 Kannatey-Asibu, Jr., E., "The Metal Cutting Optimal Control Problem—A State Space Formulation," *Control of Manufacturing Processes and Robotic Systems*, ASME Booklet, Nov. 1983, pp. 65-77.

24 Askill, J., "Radioactive Tracer Diffusion Data in Metals, Alloys, and Oxides," *Tracer Diffusion Data for Metals, Alloys and Simple Oxides*, Plenum, New York, 1970, pp. 27-81.

25 "Properties and Selection: Irons and Steels," *Metals Handbook*, ASM, Vol. 1, 1978.

26 "Properties and Selection: Stainless Steels, Tool Materials, and Special Purpose Metals," *Metal Handbook*, ASM, Vol. 3, 1978.